Spring 2009

An investigation of the combustion of oil sand derived bitumen-in-water emulsions

Timothy Robert Kennelly
University of Iowa

AN INVESTIGATION OF THE COMBUSTION OF OIL SAND DERIVED BITUMEN-IN-WATER EMULSIONS

by

Timothy Robert Kennelly

A thesis submitted in partial fulfillment
of the requirements for the Master of
Science degree in Mechanical Engineering
in the Graduate College of
The University of Iowa

May 2009

Thesis Supervisor: Professor Lea-Der Chen

Graduate College
The University of Iowa
Iowa City, Iowa

CERTIFICATE OF APPROVAL

_____

MASTER'S THESIS

_____

This is to certify that the Master's thesis of

Timothy Robert Kennelly

has been approved by the Examining Committee for the thesis requirement for the Master of Science degree in Mechanical Engineering at the May 2009 graduation.

Thesis Committee:_____
Lea-Der Chen, Thesis Supervisor

_____
Albert Ratner

_____
Shaoping Xiao

ACKNOWLEDGEMENTS

The author would like to thank Professor L. D. Chen for all his support and guidance throughout the development and preparation of this thesis. His support and guidance has been instrumental in my ability and desire to perform research in the area of combustion sciences. Professor Albert Ratner for the use of his high-speed camera. I would also like to thank Neil Buckney and my younger brother Patrick for their assistance in the laboratory in obtianing the data necessary for this thesis. I would like to thank Randall and Barbara Meyer whose generous scholarship contribution helped fund my post-graduate education associated with this thesis. Fourthly, I would like to thank my parents Patrick and Juli and my older brother Ryan for supporting me in my path to obtain higher education. Finally, I would like to thank the sponsor of my research Quadrise Canada Corporation for supporting this research and supplying their products that were necessary to perform the research.

ABSTRACT

Dwindling conventional oil resources has caused exploration efforts to focus elsewhere. Bitumen from oil sands has emerged as one of the primary unconventional oil resources in use today. Quadrise Canada Corporation has harnessed this unconventional oil by developing their bitumen-in-water emulsion known as MSAR (Multi-Phase Superfine Atomized Residue). Fuel-in-water emulsions are linked to a combustion phenomenon known as micro-explosion, which are associated with an increase in combustion efficiency and decrease in harmful emissions. A study has been conducted of the MSAR fuel to help advance the optimization and modeling of its use in spray combustors so as to best harness the potential. Quantitative and qualitative data has been obtained during combustion experiments of the fuel that will attribute to this end. Additionally, a simplified statistical model is presented based on the governing equations to describe the atomization that occur as a result of micro-explosions of the MSAR fuel as well as a simple model to represent internal force needed for a micro-explosion to occur. The results of this study continue to reinforce the understanding that micro-explosions cannot be attributed to one overriding physical principal, but rather are th result from variations in turbulent, dynamic, and thermal forces.

TABLE OF CONTENTS

LIST OF TABLES

LIST OF FIGURES

CHAPTER 1 **:** INTRODUCTION

The United States consumes more oil than any other nation in the world. In 2005 alone the United States consumed just under 7.6 billion barrels of crude oil (U.S. total Crude Oil EIA, 2006). This rate of consumption is not sustainable. M. King Hubbert is attributed to predicting the "insustainability" of crude oil production in his paper entitled *Nuclear Energy and Fossil Fuels*. He predicted in 1956 that United States oil production would peak between the late 1960s and early 1970s (Wikipedia, 2007). United States crude oil production peaked in 1970. While much attention was given to the U.S. oil production peak, another major oil producing nation, Venezuela, whose oil production also peaked in 1970 was overlooked despite the event having the same predictive consequences. The two North Sea producers, the United Kingdom and Norway, saw peak production in 1999 and 2000 respectively (Brown, 2006). Although, the first heated debate over peak oil production, which took place in the U.S. is over, the debate over when the world oil production will peak still rages. The inability to predict future oil reserve discoveries, the uncertainty involved with known reserve estimates and technology makes coming to a consensus on a date for world oil peak production seemingly impossible. Nonetheless there is a consensus that world crude production will ultimately peak and begin a steady decline. Hubbert stated in his 1981 paper entitled *The World's Evolving Energy System* , "The United States has historically been the world leader in petroleum exploration and production technology. Also during most of its history, the United States has been the leading oil producing country in the world" (p. 1015). Hubbert's comment awakens us to the fact that as the world's oil producing nations "catch up" to the United States' level of productivity and technology they will

suffer the same fate as the United States. Thus, one can argue we only have to look to the U.S to predict how declining oil production will proceed in the rest of the world. Furthermore, it is not intuitive to limit the discussion of crude oil to production; there must also be the discussion of crude oil consumption. Consumption finger pointing has already been starting to shift towards China and India as they head down socioeconomic paths that will make them the world's next largest oil consumers surpassing the U.S.

Since 1970 there has been a steady decline in U.S. domestic oil production. Figure 1-1 below shows a history of U.S. annual crude oil production.

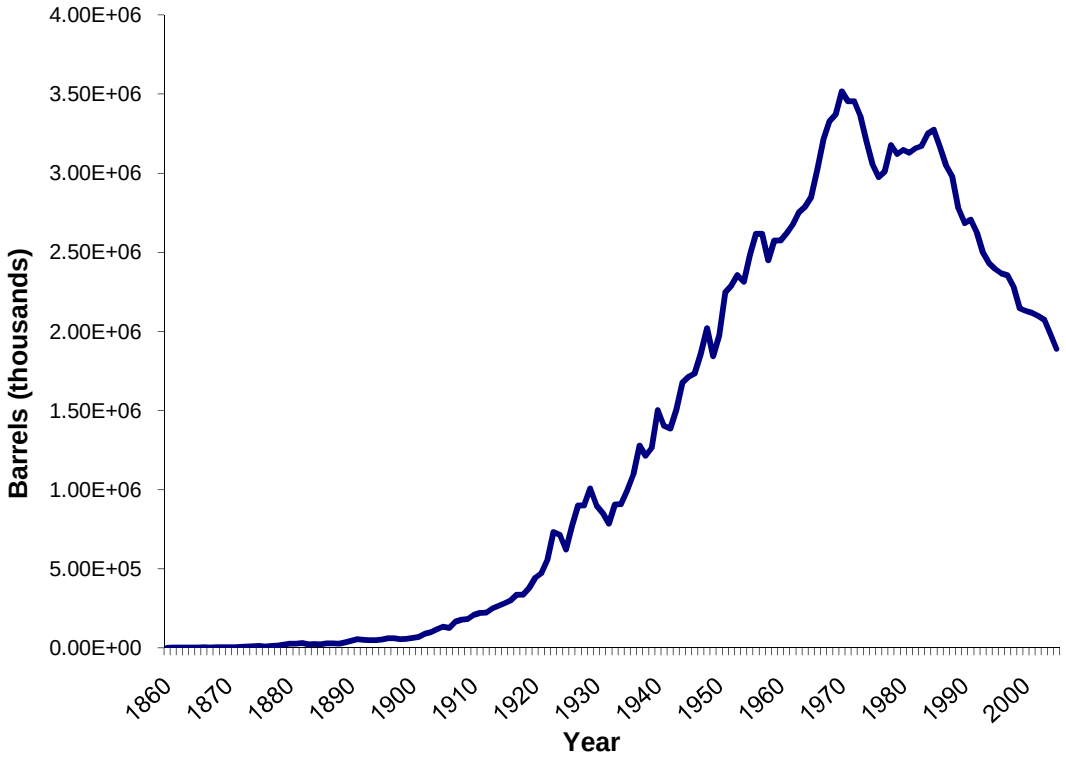

Figure 1-1: U. S. Crude Oil Production 1860-2006

Source: U.S. Energy Information Administration (EIA), 2006

Despite the domestic production decline, U.S. oil consumption continues to rise. Figure 2 below shows a recent history of U.S. oil consumption.

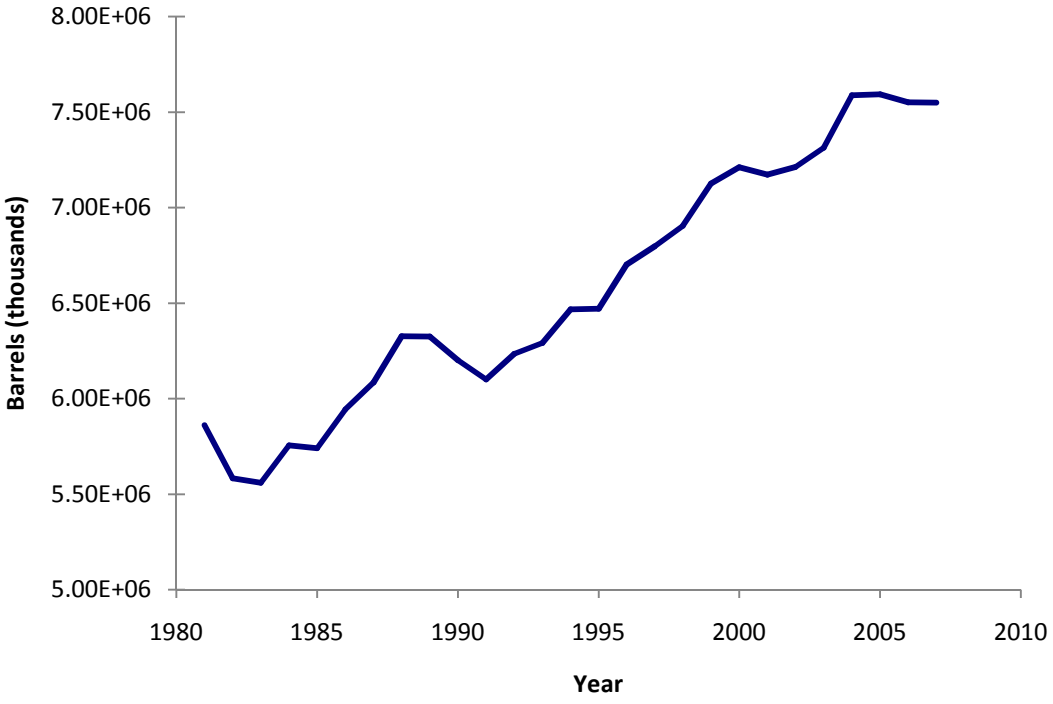

Figure 1-2: U.S. Oil Consumption 1981-2008

Source: EIA, 2009

These two trends have had the overall consequence of increasing the United States crude oil imports drastically since about 1980. Figure 1-3 is a history of U.S. crude oil imports.

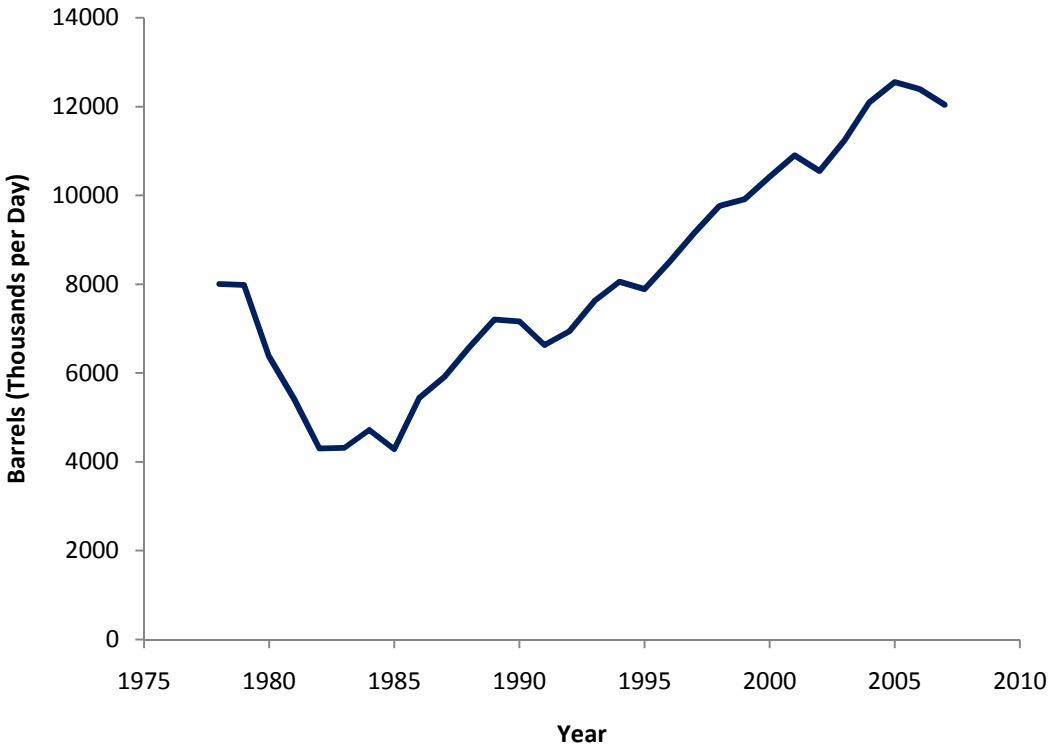

Figure 1-3: U.S. Crude Oil Imports 1971-2008

Source: EIA, 2009

In 2005 imports accounted for 59.8% of the U.S. oil consumption. Contrary to popular belief the majority of U.S. imports no longer come from OPEC nations. Beginning in 1993 the number of oil imports to the U.S. from non-OPEC nations surpassed the number from OPEC. In fact in 1996 Canada became the number one exporter of crude oil to the United States surpassing Saudi Arabia (EIA, 2006).

The largest sector for crude oil consumption in the United States is the transportation industry. Not only is the transportation industry the largest oil consuming sector, it is also the largest energy end user. Additionally the rate at which the transportation industry is consuming energy is increasing. Vehicle miles of travel (VMT)

are growing at an annual rate of 2.5% in the U.S., which is twice the rate of population growth (Sinha, 2006). Figure 1-4 below shows energy usage by sector in the United States.

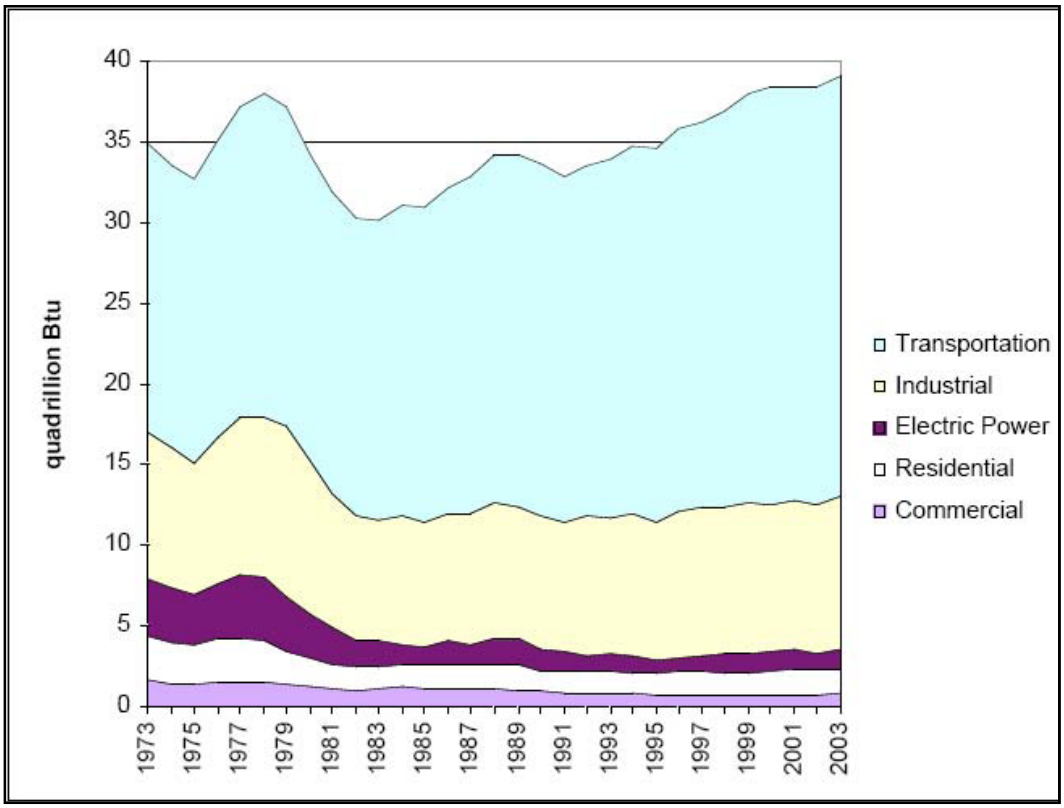

Figure 1-4: U.S. Energy Usage by Sector 2004

Source: Barker, William G. (2006). Gasoline Prices, Macroeconomics and Sustainable Transportation. *85th Annual Meeting of the Transportation Research Board* Washington, D.C January 24, 2006.

It can be seen from figure 1-4 that the transportation sector's energy usage is even well above second place industry's. Globalization of the world's economies is evidence that the need and desire for faster and more versatile transportation will continue and the demand to transports peoples and products will continue to increase. How to sustain these trends has been hotly debated. Whether centralization or decentralization results in

less transportation needs has not even been decided. Some argue that there is a direct correlation between population density and fuel consumption, while other say fuel consumption is a function of population's life patterns and travel behavior (Shim et. al). Whether or not life patterns, travel behavior, or population density changes occur the need to fuel the automobile will still be there.

Unlike the electrical grid, the transportation industry has limited fueling alternatives to power it. In particular fueling the personal automobile in the future presents the largest dilemma. A disturbing trend shows that those countries that invested the most in public transportation where the ones to see the most growth in automobile ownership (Hall, 1996). Personal vehicle use accounts for 84% of the energy consumed by transportation in the U.S. (Greene and Decicco, 2000). Thus, despite efforts to minimize automobile use the consumer is clearly more attracted to the freedom of choice the automobile brings to travel. So doing away with the personal automobile seems to be taken off the list of choices. Thus, the solution must be to find alternatives to supplement declining crude oil supply. In 2000 the transportation industry was 97% dependent on petroleum for fuel (Greene and Decicco, 2000). First and foremost supplementing declining crude oil supply must begin with improved efficiency so as to decrease the demand. Biofuels are probably the most promising alternative, however there is much concern that switching to biofuel to supply the entire mobile fuel demand would be trading one non-sustainable source of fuel for another; the argument being that there is not enough agricultural acreage to supply the food and fuel demands of the population. Additionally there is the fear that food and biofuel prices would skyrocket as supply no longer meets demand in both sectors. For the time being biofuels offer a way to

supplement the transportation industry's fuel demands, but it is yet to be seen that they will be able to fill the void declining oil production will bring. There must be another alternative that can supplement the transportation industry's fuel needs. Hydrogen fuel is another alternative but in the near term there is neither the infrastructure nor the technology to supplement gasoline as a transportation fuel. The electric vehicle is another alternative, but battery technology has not yet proven to have the storage capacity to meet travel mile needs. These fuel options and other supplemental fuels will need to be made economical to buy time for research and development towards the ultimate solution of a hydrogen fueled economy.

One of these other supplemental fuels is unconventional oil. The main sources of unconventional oil are oil shale and oil sands, respectively. This thesis will be ultimately be concerned with the unconventional heavy oil known as bitumen derived from the Canadian oil sands. However, there are two major proven reserves of oil sands: the Orinico Belt of Venezuela and the Athabasca, Peace River and Cold Lake regions of Alberta, Canada (Forouq Ali, 2002). It is estimated that 300 billion barrels of recoverable bitumen reside in Alberta, making it the largest oil reserve in the world (Masliyah et al., 2004). The ability to harvest this potential oil reserve would drastically alter the geopolitical situation giving rise for the potential of the reserves to decrease the United States' dependence on foreign oil from unstable nations. Bitumen has already proven its ability to supplement conventional crude in the form of synthetic crude oil (SCO), which can be further refined to produce conventional transportation fuels, e.g., gasoline and kerosene. Furthermore, bitumen can be emulsified with water to produce viable fuels such as Orimulsion 100 and 400, which have proven to be effective fuels for

stationary combustors (Bitumenes Orinico, 2006). Research, however, is just beginning to determine the applicability of using these types of fuels in the diesel engine. This thesis will hopefully contribute to the effort of providing the knowledge and the motive to further advance their use in atomize spray combustors.

1.1 Bitumen

Oil sands consist of three main components: bitumen, water, and a combination of quartz sand and clay mineral as illustrated in Fig. 1-5, taken from Czarnecki et al. (2005).

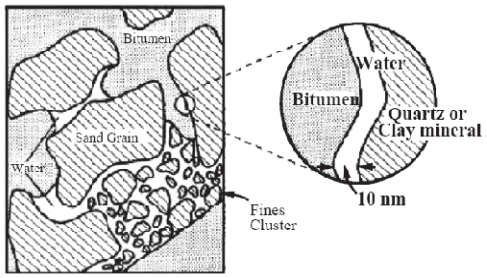

Figure 1-5: Illustration of the structure of Athabasca Oil Sands

Source: Czarnecki J., Hamza H., Masliyah J., Xu ZH, & Zhou ZJ. (2004). Understanding water-based bitumen extraction from Athabasca oil sands. *Canadian Journal of Chemical Engineering*, 82 (4), 628-654.

.

Seventy-five to eighty percent is inorganic material, with ninety percent of the inorganic material being composed of quartz sand, 3 to 5 percent water, and 10 to 12 percent bitumen, with bitumen saturation varying between zero and 18 percent by weight (National Energy Board, 2004).

Bitumen itself is composed of high aromatic compounds, resins, and asphaltenes; it typically has a high viscosity, high C/H ratio, but similar specific heating value per unit

mass of fuel as conventional petroleum fuels. Tables 1-1 and 1-2 below list the physical and chemical properties for selected Athabasca and Cold Lake bitumens.

Table 1-1: Properties and SARA Fractionation Results for Athabasca and Cold Lake Bitumens

	Athabasca	Cold Lake
API gravity	8.05	10.71
viscosity at 24 °C (Pa•s)	323	65
saturates (wt %)	17.27	20.74
aromatics (wt %)	39.70	39.20
resins (wt %)	25.75	24.81
asphaltenes (wt %)	17.28	15.25
carbon (wt %)	83.34	83.62
hydrogen (wt %)	10.26	10.50
sulfur (wt %)	4.64	4.56
oxygen (wt %)	1.08	0.86
nitrogen (wt %)	0.53	0.45
residue (wt %)	0.15	0.01

Source: Permanu, Subodhsen, Barry B. Pruden, & Parviz Rahimi (1999). Molecular Weight and Specific Gravity Distributions for Athabasca and Cold Lake Bitumens and Their Saturate, Aromatic, Resin, and Asphaltene Fractions. *Ind. Eng. Chem. Res.*, *38,* 3121-3130.

Table 1-2: Molar-Average Molecular Weights of Athabasca and Cold Lake Bitumens and Their SARA Fractions Using VPO

	Athabasca	Cold Lake
bitumen	557	550
saturates	381	378
aromatics	408	424
resins	947	825
asphaltenes	2005	1599

Source: Permanu, Subodhsen, Barry B. Pruden, & Parviz Rahimi (1999). Molecular Weight and Specific Gravity Distributions for Athabasca and Cold Lake Bitumens and Their Saturate, Aromatic, Resin, and Asphaltene Fractions. *Ind. Eng. Chem. Res.*, *38,* 3121-3130.

Bitumen's first boiling fraction boils at 245°C (Marcano et al., 1990).

Bitumen also has high trace metal compositions, e.g., 440 ppm vanadium, 110 ppm Ni, 40 ppm sodium, 12 ppm iron, high sulfur content of 4.04%, and 0.12% ash. Trace Metal composition of Cero Negro bitumen from the Orinoco Belt region of Venezuela are given in Table 1-3 (taken from Miller and Srivastava, 2000). Schutte et al. (1999) give a further break down of bitumen's trace properties, however in this instance the bitumen is that of the Canadian Oil Sands. The results of their work can be found in Table 1-4.

Table 1-3: Typical Properties of Cero Negro Bitumen

Property	Value	Property	Value
Carbon (%)[a]	85.3	° API[b]	8.0
Hydrogen (%)	9.7	Viscosity (mPa s at 25°C)	8×10^{4}–10^{5}
Nitrogen (%)	0.54	Density (kg/m^3 at 15°C)	1.019
Oxygen (%)	0.30	Gross heating value (MJ/kg)	42.8
Sulfur (%)	4.04	Flash point (°C)	120
Ash (%)	0.12	Pour point (°C)	38
Sodium (ppm)	40	Saturates (%)	10.7
Vanadium (ppm)	440	Aromatics (%)	58.0
Nickel (ppm)	110	Resins (%)	19.3
Iron (ppm)	12	Asphaltenes (%)	11.9

[a] Percentages are weight percentages, unless otherwise noted.
[b] American Petroleum Institute.

Source: Miller, C. A. and Srivastava, R. K., 2000, The combustion of Orimulsion and its generation of air pollutants. *Prog. Energy Combust. Sci*., 26, 131-160.

Table 1-4: Trace Metal Concentrations in Athabasca Bitumen

Average concentration of elements in fractions from 10 oil sands												
Size, µm	Ti	V	Al%	Ca%	Dy	Sm	Ba	Eu	Na	Mn	K	Cl
<3.9	5270	109.0	11.20	0.195	4.62	8.0	358	1.40	10900	421	14800	5420
3.9–7.8	5810	88.4	9.02	0.193	5.45	9.1	421	1.66	1030	825	14800	76
7.8–31	5550	51.3	4.68	0.128	5.62	7.6	393	1.16	757	304	13200	79
31–45	6430	29.0	2.18	0.072	5.90	5.5	359	0.99	599	130	10600	35
45–90	4420	22.6	1.83	0.041	4.83	6.9	313	0.95	532	94	8670	34
90–150	1620	8.0	0.83	0.016	1.41	3.0	168	0.32	249	34	3510	26
150–180	500	4.4	0.68	0.016	0.86	1.7	140	0.19	198	26	2590	30
180–250	867	11.0	1.22	0.099	1.14	2.4	187	0.27	985	102	4310	48
>250	2970	40.3	2.93	0.332	2.92	4.1	222	0.60	693	359	6690	195
Standard deviation of average element concentration												
Size, µm	Ti	V	Al%	Ca%	Dy	Sm	Ba	Eu	Na	Mn	K	Cl
<3.9	1250	22.7	1.94	0.079	1.73	4.0	80	0.64	7990	186	4150	8570
3.9–7.8	1140	10.3	0.75	0.046	2.05	4.4	61	0.70	169	409	1590	63
7.8–31	831	8.8	1.61	0.075	1.62	3.6	171	0.53	177	113	4310	53
31–45	1280	2.2	0.57	0.030	2.35	2.3	224	0.35	270	49	6690	14
45–90	1560	4.1	0.48	0.012	2.50	3.2	145	0.41	162	23	4260	8
90–150	530	1.8	0.14	0.009	0.68	1.9	30	0.14	50	13	872	6
150–180	101	1.7	0.15	0.012	0.38	1.3	24	0.05	39	17	607	11
180–250	774	9.7	0.73	0.132	0.60	1.3	55	0.15	758	101	1580	53
>250	1650	20.8	1.56	0.668	1.33	1.9	68	0.27	349	291	2580	328
Relative standard deviation (RSD)												
Size, µm	Ti	V	Al%	Ca%	Dy	Sm	Ba	Eu	Na	Mn	K	Cl
<3.9	0.24	0.21	0.17	0.41	0.37	0.50	0.22	0.46	0.74	0.44	0.28	1.58
3.9–7.8	0.20	0.12	0.08	0.24	0.38	0.49	0.14	0.42	0.16	0.50	0.11	0.82
7.8–31	0.15	0.17	0.34	0.59	0.29	0.47	0.44	0.46	0.23	0.37	0.33	0.67
31–45	0.20	0.08	0.26	0.42	0.40	0.42	0.62	0.36	0.45	0.37	0.63	0.39
45–90	0.35	0.18	0.26	0.29	0.52	0.46	0.46	0.43	0.30	0.25	0.49	0.23
90–150	0.33	0.22	0.17	0.54	0.48	0.63	0.18	0.43	0.20	0.38	0.25	0.23
150–180	0.20	0.39	0.22	0.74	0.44	0.78	0.17	0.26	0.20	0.64	0.23	0.36
180–250	0.89	0.89	0.60	1.34	0.52	0.52	0.30	0.56	0.77	0.99	0.37	1.11
>250	0.56	0.52	0.53	2.01	0.45	0.47	0.31	0.44	0.50	0.81	0.39	1.68
Avg. RSD	0.35	0.31	0.29	0.73	0.43	0.53	0.32	0.42	0.40	0.53	0.34	0.79

Source: Schutte, Robert, Gordon R. Thompson, Kingsley K. Donkor, M. John M. Duke, Cowles, Xiu Ping Li, & Byron Kratochvil (1999). Estimation of particle size distribution in Athabasca oil sands by indirect instrumental neutron activation analysis. *Can. J. Chem.*, 77, 1626–1637.

1.2 MSAR

In the early 1990s, Quadrise Canada Corporation was founded with the development of their emulsified fuel known as MSAR. The acronym stands for Multiphase Superfine Atomized Residue. MSAR is an oil-in-water emulsion: Canadian bitumen represents the dispersed phase, while water comprises the continuous phase.

However, Quadrise has not limited production to using water as the continuous phase; their latest version of the fuel uses two volatile hydrocarbons as the continuous phase in place of water. Three of Quadrise's MSAR fuels are investigated in this study: a) a 30% water emulsion, b) a 20% water emulsion and c) a 30% PPA/HFO emulsion. The emulsifying process and the surfactants used in the development of MSAR are Quadrise Fuel International's trade secrets, thus, a detailed discussion of the fuel and surfactant cannot be provided here. Quadrise does provide information, however, on the internal phase size distribution of the micro-dispersed bitumen droplets within the fuel which are between three and five microns. Figure 1-6 is a micrograph from Quadrise of a typical 80-100 micron MSAR droplet residing next to a typical heavy fuel oil droplet. An MSAR droplet has 17x greater surface area, i.e., burning area compared to a heavy fuel oil droplet as consequence of the micro-dispersed bitumen droplets.

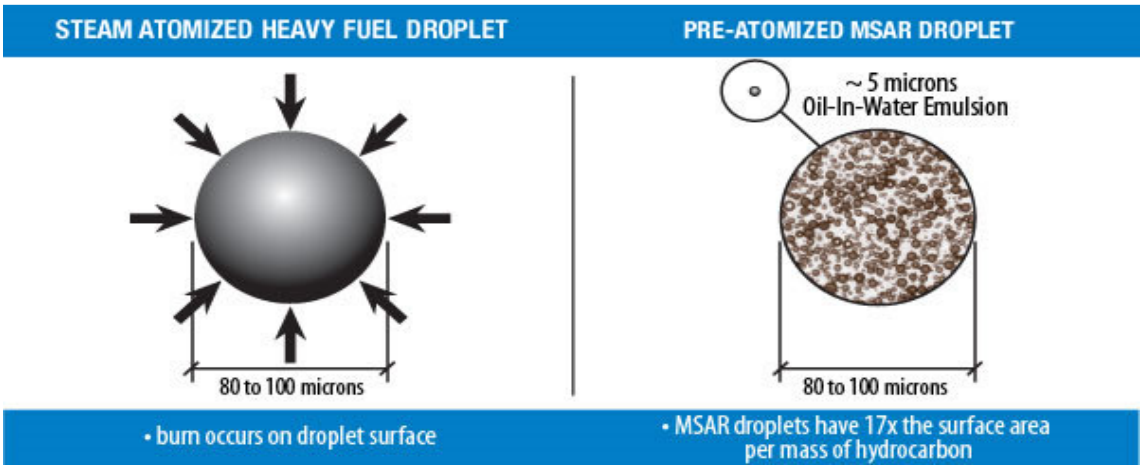

Figure 1-6: Typical Heavy Fuel Atomized Droplet (Left) and an MSAR droplet (Right)

Source: Quadrise Canada Corporation (2007). What is MSAR? *Quadrise Limited.* Retrieved December 27, 2007 from http://www.quadrisecanada.com/msar.html.

1.3 Fuel Droplet Combustion

A discussion of liquid fuel droplet combustion must coincide with a discussion of liquid droplet vaporization. The basic droplet combustion model to initially make this comparison is accredited to Godsave and Spalding in the 1950s (Law, 1982). It was determined that droplet vaporization and combustion of a pure liquid droplet are fundamentally the same. Simply put, the only real distinction between combustion and vaporization of a liquid droplet is in the fact that during combustion an enveloping flame acts as a high-temperature pressure chamber surrounding the liquid droplet, while during vaporization the liquid droplet is merely enveloped by a vapor region that is at a much lower temperature and pressure than that of the flame. Thus, in making this distinction it is assumed that pyrolysis of fuel vapors during combustion, neglecting pressure and temperature differences, has no consequence on the vaporization rate of the liquid droplet. Whether considering the regression of the droplet during evaporation or the rate of fuel consumption during combustion the same modeling theory applies (Kuo, 1986). The widely accepted law that defines this principle is the d^2 law, which has been verified experimentally:

$$d^2 = d_o^{\,2} - \beta_\upsilon t$$

(1)

where d is the droplet diameter after time t, d_o is the initial droplet diameter, and β_v is what is known as the evaporation coefficient. The law asserts that mass is continuously fed to the droplet surface from the interior of the droplet by means of diffusion until the droplet is completely vaporized or combusted and d equals zero. The heat flux at the surface of the droplet determines the rate of regression (Kuo, 1986). Although, there are

many assumptions associated with the d^2 law, e.g., the droplet must be geometrically spherical, they will not be discussed here; for a complete discussion of the d^2 law refer to Law (1982). Before we end the discussion it must be noted that generally speaking the temperature at the center of the droplet is much lower than the temperature at the surface, although with time a temperature may be reached before complete evaporation of the droplet known as the "wet bulb" temperature in which all remaining heat transfer is in the form of latent heat (Faeth, 1977). Although, the d^2 law is a great basis at which to start with for a back of the envelope type calculation, as we will soon find out combustion is a complex phenomenon involving extensive analysis in the areas of fluid mechanics, heat and mass transfer, and chemical kinetics.

In addition to the d^2 there are also many more complex models that take into the account droplet liquid-phase internal circulation. Internal circulation within the droplet is induced by shear stresses at the droplet surface due to gaseous forced and natural convection (Law, 1982). An extremely thin liquid and a larger gaseous boundary layer are formed at the surface of the droplet resulting in a wake region in the direction of the convective flow; the result is the formation of internal vortices (Kuo, 1986). Internal circulation will affect the evaporation rate of the droplet. The greater the momentum of the vortices below the surface of the droplet, the greater rate of heat transfer from the exterior of the droplet to the interior of the droplet, thus slowing evaporation at the surface by decreasing the temperature at the surface. A pure conductive model with zero internal circulation would not experience these effects, however if during the lifetime of the droplet the droplet reaches an equilibrium temperature (wet-bulb temperature), these effects would no longer be applicable as well (Kuo, 1986).

In the 1960s Ivanov and Nefedov began experimenting with the fuel droplet combustion of “mixtures” of immiscible liquids (Ivanov and Nefedov, 1965). Ivanov and Nefedov placed a water-in-mazut emulsified droplet on a quartz filament and inserted the droplet into a high-temperature chamber environment where the particle was allowed to auto-ignite. The combustion was filmed using high-speed cinematography at 200-300 fps. They found through these experiments that the principles governing pure liquid and miscible liquid mixture evaporation and combustion did not align with that of emulsified fuels. They labeled the uncharacteristic burning of emulsified fuel droplets “micro-explosion”. Ivanov and Nefedov’s motivation to study the combustion of an emulsified fuel stemmed from the fact that the evaporation of a fuel is faster in humid air than it is in dry air. Like Ivanov and Nefedov’s experiments most attention since their discovery has been paid to water-in-oil (W/O) emulsions. Others including this thesis have more recently begun to give more attention to oil-in-water emulsions (O/W). However, a discussion of W/O emulsions will persist first.

The benefits of micro-explosion and the addition of water to fuel are well documented in the literature. These benefits include reduction in NO_x, reduction in particulate matter and soot, and reduction in unburnt hydrocarbons and PAHs (poly-aromatic hydrocarbons), which is all accompanied by a faster and more complete combustion of the fuel resulting in greater efficiency. The reduction in temperature associated with these advantages, e.g., NO_x reduction, should also not go unmentioned for its ability to reduce cooling needs of the combustor, and in terms of the IC engine increase the compression ratio. The reduction of soot and unburnt hydrocarbons in addition to its environmental implications will also prevent the fouling of boilers and

furnaces. As Dryer (1977) points out theses advantages stem from combination of both physical and chemical kinetic effects as a result of emulsifying water in fuel. As has been made apparent micro-explosion has evolved as the word to describe the physical phenomenon taking place. Micro-explosion is characterized by the ejection of vapors and secondary droplets at the original fuel droplet's surface. Micro-explosion has been described as a form of secondary atomization that is created by means of droplet internal conditions and physical structure rather than surface conditions associated with convective shear stresses as the term is formally used, e.g., when using the Weber number to predict breakup (Law, 1977). A more recent description by Zeng et al. describes micro-explosion as the fragmentation of liquid droplets due to violent internal gasification (2007).

Following the practical example of Ivanov and Nefedov, many have used a filament or thermocouple to suspend the emulsified droplet, but as Dreyer (1977) points out the use of a filament or a thermocouple to suspend the emulsified droplet during experiments will result in coalescence of water at the metal surface, thus altering the physical structure of the emulsified droplet. Dryer proposed that this would inhibit micro-explosion, but there is much evidence to contradict this conclusion. However, probably more importantly, Dryer also pointed out that this will impede treating the nucleation of the fuel as strictly homogeneous (1977). Boiling temperatures of a liquid are based on the initiation of nucleation of that liquid in contact with a surface (heterogeneous nucleation), while the limit of superheat is another nucleation temperature of a liquid that lies well above that of the heterogeneous boiling point and is defined at the ideal condition in which the liquid is not in contact with any surfaces (homogeneous

nucleation). Thus, it has been postulated by Dryer and others that reaching limit of superheat of the trapped micro dispersed water droplets in W/O emulsion is one of the main criteria to be reached for the onset of micro-explosions in these fuels.

Another approach to micro-explosion as Law points out is to look at it in terms of the differences in volatilities of the two liquids being emulsified (which relates back to the superheat argument); most practical fuels in use today have a much lower volatility than that of the water they are being emulsified with (Law, 1977). Thus, the higher volatility liquid (water) trapped by the lower volatility liquid (fuel) will rupture, while the lower volatility liquid is still in its heating stage. Law (1977) also points out that the vaporization of water reaching the droplet surface will cool the droplet preventing soot precursors from forming and reducing the formation of carbonaceous residue. Sooting/coking will also be reduced due to the reduction in droplet lifetime as a result of micro-explosion, i.e., increased burning rate. Furthermore, the presence of water in W/O emulsions results in an increase in OH radicals, which have been shown to oxidize soot precursors (Dryer, 1977). The 1977 paper by Law was also the first attempt to theoretically model W/O emulsion combustion based on the thermodynamic limit of superheat.

Lasheras et al. experimented with free droplet combustion to avoid the heterogeneous nucleation affects postulated by Dryer (1979). Laheras et al. injected a fuel droplet into a vertical oriented high-temperature gas flow. The fuels used were n-dodecane, n-tetradecane, and n-hexadecane. Avedesian and Adres predicted through kinetic approaches that micro-explosion would not occur unless the fuel had a higher boiling point than the superheat limit of the internal phase water droplets (1978). The

superheat limit of water is between 277°C and 307°C (Law, 1977). N-dodecane, n-tetradecane, and n-hexadecane have boiling points of 216, 252, and 287°C, respectively (Lasheras et al., 1979). Lasheras et al. did in fact find that n-tetradecane and n-hexadecane micro-exploded, while n-dodecane did not. The water content of the emulsions were also varied and it was determined that water concentration plays a pivotal role in determining the severity of micro-explosion. Finally, Lasheras et al. noted that temperature data at the droplet surface did not align with the assumption that water vaporization is steady and continuous at the surface, and thus hypothesized that water vaporization within an emulsified droplet must be inhibited in some way (1979).

Law et al. (1980) studied the effects of droplet internal circulation on W/O emulsion combustion. It was determined that the minimization of droplet internal circulation will increase the intensity of micro-explosion and that internal circulation may even prevent micro-explosion from occurring. Internal circulation will allow for water to reach the surface of the emulsified droplet and vaporize before the limit of superheat of the micro-dispersed water droplets can be reached and homogeneous nucleation initiated. The pure convective model (infinite internal circulation) and pure conduction model (zero internal circulation) are sometimes referred to the distillation and frozen mode, respectively. Another contributing factor to the likelihood and intensity of micro-explosion is pressure; increasing pressure will raise the boiling points of the emulsified components, while the limit of superheat of water remains constant, thus increasing the intensity of the micro-explosion phenomenon (Wang et al., 1984). Wang et al. also found evidence that micro-explosion may also be affected by the way in which a fuel droplet is generated, i.e., spray atomization techniques could enhance or inhibit micro-explosion.

Other referenced work that has contributed to the W/O emulsion discussion include: Avedisian and Glassman (1981); Cho et al. (1991).

Researchers have qualitatively observed differences in the combustion behavior of O/W emulsions as opposed to W/O emulsions. In O/W emulsions, water is the continuous phase, while the fuel is the dispersed. Williams and Porkashanian (1987) investigated the combustion behavior of bitumen-in-water emulsions as opposed to coal-water slurries and medium fuel oil. They found that the micro-explosion phenomenon associated with bitumen-in-water emulsions differed greatly with the splattering that is normally associated with coal-water slurries and heavy oil. The bitumen-in-water emulsions were found to have a maximum temperature of 1739K right before the rupturing of the droplet, while coal-water slurry and medium fuel oil had a maximum droplet temperature of 1648K and 1723K, respectively (Williams & Porkashanian, 1987). The ignition delay time for bitumen-in-water emulsions is also shorter than for coal-water slurries (Williams & Porkashanian, 1987). Thus, it is clear from Williams and Porkashanian's initial work that bitumen-in-water emulsions are generally speaking a better fuel than fuel oil and coal-water slurries. Additionally, in terms of these advantages the easier handling and transportation of bitumen/heavy oil-in-water emulsion should not go unmentioned because of the reduced viscosity associated with water addition.

Marcano et al. (1990) performed a combination of suspended, free-falling, pyrolysis and spray combustion experiments on bitumen-in-water emulsions in a hot-temperature gas environment. The bitumen was obtained from the Orinoco Belt of Venezuela. Four samples were tested: 1) Orimulsion 100, 2) neat bitumen, 3) self-prepared bitumen-in-water emulsions of 10, 18, 24 and 35 % volume water with a 0.5

mass % commercial surfactant and 4) a hard petroleum bitumen slurry. The neat bitumen and hard bitumen slurry did not display the same disruptive burning effects as the self-prepared bitumen-in-water emulsions and Orimulsion. Additionally, the disruptive burning of the bitumen-in-water emulsions resulted in no carbonaceous residue being left behind. Water addition increased the ignition delay time of the fuels especially in amounts greater than 24%, however ignition delay was only slightly affected with furnace temperatures >1123K. Moving on, Namba and Kimoto (2000) investigated the combustion of asphalt-in-water emulsions suspended in a high temperature furnace; they found that the emulsion droplet often displayed micro-explosive behavior at a furnace temperature of 1073K, but displayed violent micro-explosions at 1173K. They also found that ignition delay appeared to be uninhibited at high temperatures, however, at lower temperatures droplet diameter was a variable effecting ignition delay times with ignition delay increasing with increasing diameter (2000). It is important to note that bitumen/asphalt emulsions are found to have grater micro-explosion intensities compared to the n-alkane emulsions of previous work, this is believed to be do to the higher viscosity of the heavy oils compared to the n-alkanes. The higher viscosity of the heavy oil emulsions decreases internal circulation of the droplets providing for higher energy nucleation sites to develop and consequently causing violent micro-explosions to occur. A thicker fuel shell, to be discussed later, is also considered to be a reason for this difference in mircro-explosive intensity. Marcano et al. (1990) categorizes the combustion of bitumen-in-water emulsion combustion into three steps which will be presented here:

1. The pre-ignition stage during which the droplet is heated and evaporation of the volatile material begins followed by pre-ignition swelling in which the initial droplet (d_o) diameter increases to d_i. This stage ends with the self-ignition of the vapor surrounding the droplet. This is characterized by a sharp rise in OH emission from the combustion of pre-vaporized material immediately followed by a yellow emission from the developing diffusion flame.
2. The combustion stage in which the volatile constituents and the cracked products burn in an envelope diffusion flame (yellow emission) surrounding the droplet.
3. The coke combustion stage which occurs after the evolution of the volatile material stops and is characterized by the coke combustion time and also monitored by the center temperature.

Namba and Kimoto (2000) also make an extremely prevalent hypothesis/qualitative observation that during the heating period (ms time-scale) the emulsion droplet is "rearranged" to form an outer shell composed primarily of the fuel (asphalt). As noted earlier, Lasheras et al. (1979) hypothesized that water vaporization must be inhibited in some way within in an emulsified droplet; this proposed surface fuel shell could be the answer Lasheras et al. were looking for, however, if we look at Segawa et al.'s (2000) work, they postulated that the shell formation phenomenon is only present in O/W emulsions, whereas Lasheras et al. (1979) studied W/O emulsions. Yet, Segawa et al. did mention that they have not proven that the same conditions are not present in a W/O type. Segawa et al. work determined that for an n-hexadecane-in-water emulsion heated under micro-gravity the dispersed hexadecane micro-droplets agglomerated and coalesced

demulsifying the O/W droplet. The separated n-hexadecane fuel formed a clear shell surrounding an opaque water-droplet center. Figure 1-7 below depicts this phenomenon.

Figure 1-7: The Phase Separation of an n-hexadecane-in-water emulsion droplet

Source: Segawa, Daisuke, Hiroshi Yamasaki, Toshikazu Kadota, Hidemitsu Tanaka, Hiroshi Enomoto, Mitsuhiro Tsue (2000). Water Coalescence in an Oil-in-Water Emulsion Droplet Burning Under Microgravity. *Proceedings of the Combustion Institute,* 28, 985-990.

Previously, Avedisian and Fatehi (1988) investigating the Leidenfrost droplet vaporization characteristics of water-in-heptane and water-in-decane emulsions on a hot surface qualitatively noticed a similar occurrence, in that the emulsion droplets before complete vaporization from the hot plate's surface went from a "milky white" color to a clear solution; at the time they could not determine the cause. Furthermore, previous

work by the same group of authors gave results that could be attributed to the formation of the fuel shell: Yamasaki et al. (1998) performed experiments in which the n-hexadecane droplet was allowed to ignite and then after some arbitrary time was quenched, and the water and fuel were separated afterwards and their quantities measuered. They determined from this that in-at-least the preliminary combustion stages before micro-explosion occurs that fuel is vaporized, while at the same time the water concentration remains fairly constant, providing quantitative evidence for the presence of a fuel shell. Finally, Tsue et al.'s 1996 work found that an n-dodecane droplet of the O/W type will micro-explode, while one of the W/O type, as previously discussed, will not. This goes against the previous postulation by Avedesian and Adres (1979) that micro-explosion will not occur unless the boiling point of the fuel is greater than that of the superheat limit of water.

Most theoretical models of W/O and O/W emulsions have focused on the probability of occurrence of micro-explosion or the rate of homogeneous nucleation bubble generation within the droplet based on the limit of superheat of water within the emulsion. As mentioned earlier Law (1977) was first to try to theoretically predict the occurrence of micro-explosion by predicting its occurrence to be at the thermodynamic limit of superheat of the micro-dispersed water droplets of a W/O emulsion. This model was found to overestimate the temperature at which the superheat limit would occur, and it was concluded a model based on chemical kinetics would be needed. Avedisian and Adres (1978) took this approach. Kadota and Yamasaki outlined the equations for the steady state rate of nucleation within a binary mixture for both homogeneous and heterogeneous nucleation. Kadota and Yamasaki (2002) through experimentation

derived an empirical equation for the rate of micro-explosion as function of temperature and water volume, the equation is presented as equation 2 below

$$J = KV_w \exp\left[\frac{A}{T_E}\right] \quad (2)$$

where K and A are empirical coefficients, V_w is the water content volume, and T_E is the emulsion temperature. The superheat limit of water is much greater than the superheat limit of water within an emulsified droplet, and thus a combination of both heterogeneous and homogeneous nucleation of water must be present. Because water nucleation is a hybrid of both nucleation processes within an emulsified droplet, Kadota and Yamasaki attempted to describe the nucleation as a probability function. In particular they used a Weibull distribution as the limiting case of the weakest link destruction model that would predict the probability of nucleation occurrence based on a shape factor, and thus the occurrence of micro-explosion. Using this model they found, despite this hybrid effect, that a quasi-linear relationship could be attributed to the rate of micro-explosion against the theoretical rate of homogeneous nucleation of a pure substance. Micro-explosion was determined to be both a function of temperature and water volume.

Fu et al. (2002) looked to establish a theoretical model for micro-explosion based on the fuel shell formation model, which they chose to refer to as the oil membrane. Fu et al. postulated that an oil membrane was formed of a thickness equal to the diameter of the micro-dispersed droplets for both O/W and W/O type emulsions. The initial outer layer of the emulsion droplet (once again equal in size to the diameter of the micro-dispersed droplets) would be vaporized, while simultaneously, the subsequent length scale layer just below the vaporizing layer would begin coalescing and agglomerating to form the oil membrane (2002). Figure 1-8 shows a depiction of Fu et al.'s postulated

mechanisms for the formation of the oil membrane for both the W/O and O/W type emulsions.

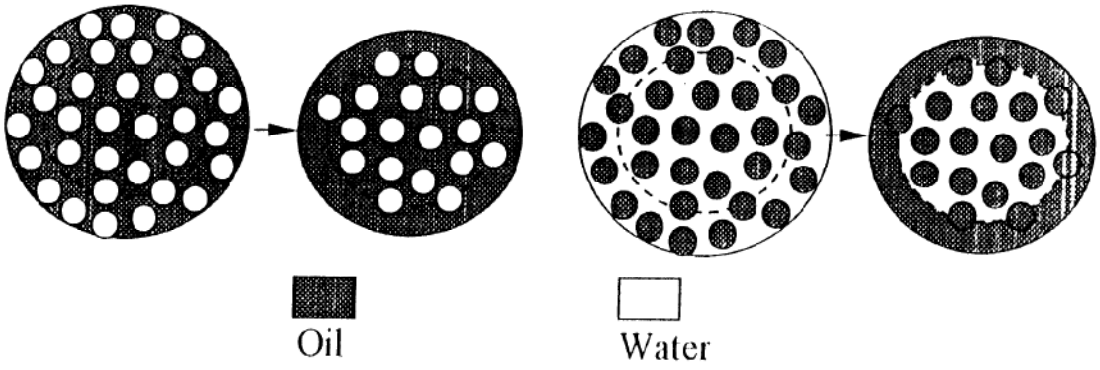

Figure 1-8: Formation of the Oil-Membrane in W/O and O/W type emulsions

Source: Fu, Wei Bia, Ling You Hou, Lipo Wang, & Fan Hua Ma (2002). A Unified Model for the Micro-Explosion of emulsified Droplets of Oil and Water. *Fuel Processing Technology.* 79, 107– 119.

Fu et al. (2002) also present a theoretical model on the combustion of O/W and W/O type emulsions based on the formation of this oil membrane. They present a three step process: 1) the inception of vaporization, 2) formation of the oil-membrane, 3) heating period in which water reaches its theoretical limit of superheat. Their function describes the intensity at which micro-explosion will occur, where, the intensity function is a function of the homogeneous nucleation rate, initial droplet radius, volume fraction of water, and micro-dispersed droplet radius. Thus, Fu et al.'s model assumes that the conditions for micro-explosion occurrence are met with the formation of an oil membrane. One variable needed to meet this criteria is the initial droplet diameter. If the initial droplet diameter is too small, their will not be sufficient volume in which to form the oil membrane, or at least one that is structurally sound to allow for the superheating

of water and subsequent nucleation (2002). Thus, micro-explosion is dependent on the ratio of micro-dispersed droplet diameter to fuel droplet diameter.

Most recently, Zeng and Lee (2007) attempted to directly describe the breakup processes of emulsified droplets through numerical simulation. Their modeling is broken up into three parts: 1) the temperature and mass fraction distribution inside the droplet, 2) bubble generation and bubble growth, and 3) breakup time and breakup outcomes. Step three is unique in its attempt to describe the velocities of and other conditions associated with the satellite droplets as a result of breakup. The basis for the simplified model is the growth of a single nucleation bubble at the center of the droplet. The model, however, does not include the formation of a fuel shell.

1.4 Specific Objectives

The objective of this thesis is to further advance the understanding of and knowledge base for the combustion of bitumen-in-water emulsions by studying the MSAR fuel. More specifically to characterize the micro-explosive properties and regimes of the fuel within different regions of a methane diffusion flame through experimentation. As part of this process this thesis wishes to document the sizes and velocities spaces of the various satellite droplets as a result of different breakup or micro-explosive regimes and document the droplet core temperature profiles present in each phase of the burning process associated with these regimes. Finally, to obtain data and present theory that will contribute to the determination of the mass burning rate of the MSAR fuel and the ongoing struggle to properly numerically model the micro-explosion phenomenon of emulsified fuels so as to contribute to the optimization of their use in atomized spray combustors.

CHAPTER 2 : DIFFUSION FLAME EXPERIMENT

2.1 Experimental Set-up

An experimental set-up was established around a methane diffusion flame to act as the ignition source to study the combustion characteristics and phenomenon of the MSAR fuel. A methane diffusion flame was chosen to quasi-simulate the use of the fuel in a furnace or boiler. The initial pressure and temperature conditions during experimentation where that of the room. A CP grade methane (99% purity) was supplied from a compressed gas cylinder. A diagram of the experimental set-up is depicted in figure 2-1 below.

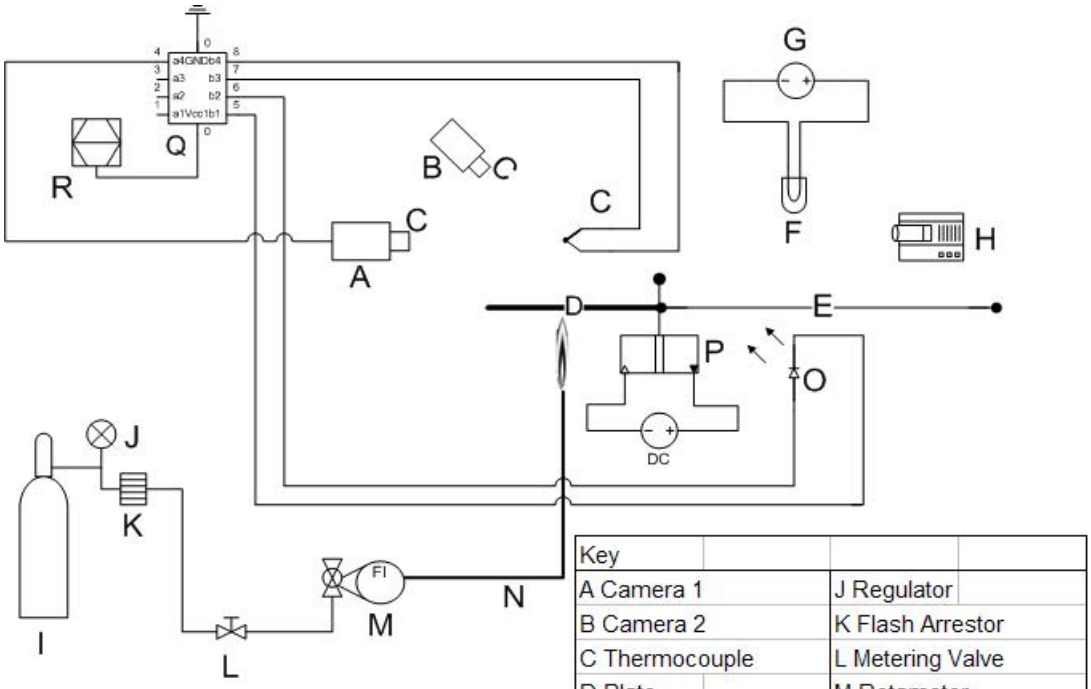

Key	
A Camera 1	J Regulator
B Camera 2	K Flash Arrestor
C Thermocouple	L Metering Valve
D Plate	M Rotameter
E Slide Mechanism	N 1/4" SS Tubing
F LED	O Photodiode
G Power Supply	P Linear Actuator
H Projector	Q Data Acquisition
I Methane Cylinder	R Computer

Figure 2-1: Schematic Diagram of Diffusion Flame Experiment

The methane exiting the cylinder was regulated using a Combustible Gas Regulator from Victor Equipment Company. As a safety precaution a flash arrestor was connected to the regulator using ¼'' stainless steel tubing. A Whitey metering valve from Swagelok was then connected to the flash arrestor. All fittings and connections were purchased from Swagelok. The metering valve was then connected to a Matheson-Trigas high accuracy rotameter (Model FM-1050 Series; 603). The rotameter's ball valve was used to regulate the flame height and velocity. Quarter inch stainless tubing (4.0 mm ID) was then strung to a Unistrut structure that held the diffusion flame. The

tubing was bent to come up from underneath the structure and held against a cross beam using brackets. The outlet of the now vertical stainless steel tubing acted as the exit nozzle to the methane diffusion flame. A ruler was secured to the Unistrut structure to measure flame height.

A mechanism was designed to initially shield the suspended fuel droplet from the flame, while the desired flame velocity could be established. A detailed discussion of the suspension of the fuel droplet will follow the discussion of the mechanism here. The mechanism consisted of a stainless steel shielding plate, a linear slide and a tension spring. The plate was a 9x9 inch square. The slide was purchased from Velmex Inc. and is part of their "Unislide" series. The slide has a transversing length of 10''. The tension spring is from KT Industries has a length of 6.5'', a 5/8'' OD, and a 0.054''wire diameter. A 150 lb linear actuator from FA Fergelli Automations was used to release the mechanism. The plate was suspended over the top of the flame by a bracket that was bolted to the slide. The mechanism was fired when a pin was released by the downward movement of the actuator, thus removing the plate, and exposing the fuel droplet to the methane diffusion flame.

The fuel droplet was suspended on the junction of a fine wire precision thermocouple. Based on the temperature range being evaluated an S-type thermocouple was chosen from Omega Engineering with a 0.003'' wire diameter having a maximum service temperature of 1450 °C and an accuracy of ± 1.5 °C. The thermocouple leads were strung through and cemented to ceramic inserts in order to handle and support the delicate thermocouple wire. The high-temperature chemically setting cement used to secure the thermocouple to the ceramic inserts was also purchased through Omega

Engineering (Omega Bond 200). The thermocouples were put in an oven at 450 °F for 8 hours to allow the cement to set.

The thermocouple junction was held over the center of the flame by a laboratory clamp by means of the ceramic insert. The laboratory clamp was able to be raised and lowered within the flame by means of a vertical transverse mechanism. The transversing mechanism allowed for the thermocouple junction to be lowered to just above the flame port so that it could be centered within the port and subsequently raised to the proper flame height to be studied; through this process the experimenter could be certain the droplet was centered within the flame. The MSAR droplets were studied at two centered heights within the flame normalized by the port diameter of 4 mm. The two normalized heights studied were 50 and 108, respectively. The 108 height was approximately that of the maximum height (18.10 in.) of the visible flame.

Two high-speed digital cameras were used for empirical observation of the combustion of the fuel droplet. The first camera was set-up with a tripod to obtain a direct shot relative to the test set-up. The second camera was positioned with a second tripod at a forty-five degree angle relative to the test set-up. The first camera is IDT's X-Stream VISION XS-3 High-speed CMOS camera. The second camera is a Casio EX-F1 digital camera. The X-Stream camera was filmed in monochrome, while the CASIO was filmed in color. A 5mm projector was used as direct backlighting for the X-Stream camera, while also providing in-direct lighting for the Casio. A Nikon lens was used in consort with the X-Stream camera for a highly magnified view of the burning droplet for an up close view of the droplet breakup. The CASIO was positioned for a wider field of view so as to see ignition and flame propagation of satellite droplets.

Data was acquired using Iotech's Personal Daq/3005. The data acquisition software used was DASYLab 8.0. The data acquisition for both the X-Stream camera and the thermocouple were triggered with the retraction of the plate. A red LED light, powered by the dual output 20V DC power supply was positioned on an electrical bread board across from a photodiode. The bread board holding the LED and the photodiode was aligned alongside the "Unislide" so that when the mechanism was fired a plate (not to be confused with the shielding plate) would travel in-between the LED and photodiode, thus blocking any light being emitted to the photodiode by the LED (See Figure 2-1). The change in light intensity resulted in a voltage drop across the photodiode, thus triggering the camera and the acquisition of temperature data from the thermocouple. Two temperature files were saved: one that started recording temperature data at the start of data acquisition and another that was triggered by the retraction of the shielding plate; having temperature data before the retraction of the plate allowed for the experimenter to adjust the timing of the experiment. A snapshot of the DASYLab WorkSheet that was generated to process the aforementioned signals from the Personal Daq is shown below in figure 2-2.

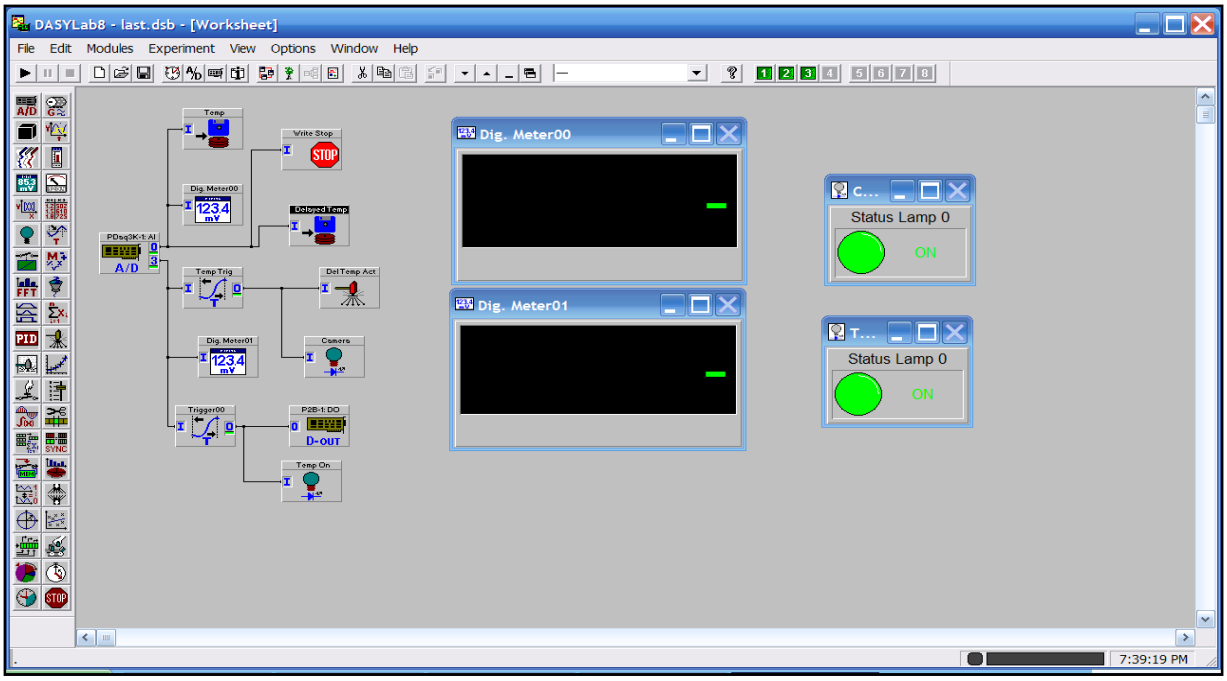

Figure 2-2: Snapshot of DasyLab Interface used in experiment

2.2 Experimental Procedure

Before an experimental run was undertaken a strict MSAR preparation procedure was followed in an attempt to achieve consistency in the fuels composition between experimental runs. Strict attention was also bad to the fact that an emulsion will demulsify over time. The bottle holding the particular MSAR sample to be studied was shaken for approximately 20 seconds and then tilted back and forth 10 times from the up-side-down position back to the upright position. The cap was then opened and a hypodermic needle was inserted into the solution approximately ¼'' below the free surface; the syringe was then filled with fuel. Droplets ranging between approximately 1.0 mm-1.6mm in diameter were then placed on the thermocouple junction using the syringe.

Experiments were performed in conjunction with a lab partner. The team followed a strict start-up procedure when igniting the methane diffusion flame. First, all valves, if not already, were closed including the metering valve and rotameter ball valve. The cylinder valve was then opened and all downfield valves and connections were subsequently checked for leaks using a leak detector solution. The cylinder valve was then closed and all downfield valves were fully opened, except for the rotameter ball valve, which was opened only one turn. A torch was then held to the flame nozzle, while the cylinder valve was opened igniting the methane gas.

Before placing a droplet on the thermocouple junction, the retracting plate mechanism was set. The cameras if not already positioned on the droplet were focused. The flame was then raised using the rotameter ball valve to the desired flame speed. The laminar flame speed was set at 8 m/s corresponding to a Reynolds number of 2119 and an average flame height of 18.1 inches. Data acquisition was then initiated, followed by the retraction of the actuator firing the plate and initiating the experimental run. After the experimental run, the flame was lowered and the process repeated pending a change in fuel or the height of droplet within the flame.

CHAPTER 3 : RESULTS AND DISCUSSION

Experimental observations point to the burning of an MSAR droplet aligning closely with the viscous shell type models of Fu et al. (2002), which were originally postulated by Kimoto and Yamasaki (2000). The reader should keep this in mind as the discussion progresses. Experimental observations also point to the fact that trapped superheated nucleation energy is in fact what eventually leads to the micro-explosion of an MSAR droplet.

3.1 Parent Droplet Breakup Regimes

Meticulous frame by frame qualitative observations of the high speed films from both the CASIO and X-Stream cameras were made of the burning droplets. From these observations the breakup of the parent droplet as a result of micro-explosions was categorized into three regimes. The author must note that there are no concrete limits that distinguish one breakup regime from the other; in many instances there maybe overlapping qualities that make one breakup regime a hybrid of another, but there is enough qualitative evidence to distinctly describe three breakup regimes. The three breakup regimes being defined are stream breakups, localized breakups and large violent breakups, respectively. The stream breakups are distinguished by the shooting out of matter from the interior of the parent droplet form a discrete location or point on the surface of the parent droplet. Figure 3-1 shows a stream breakup.

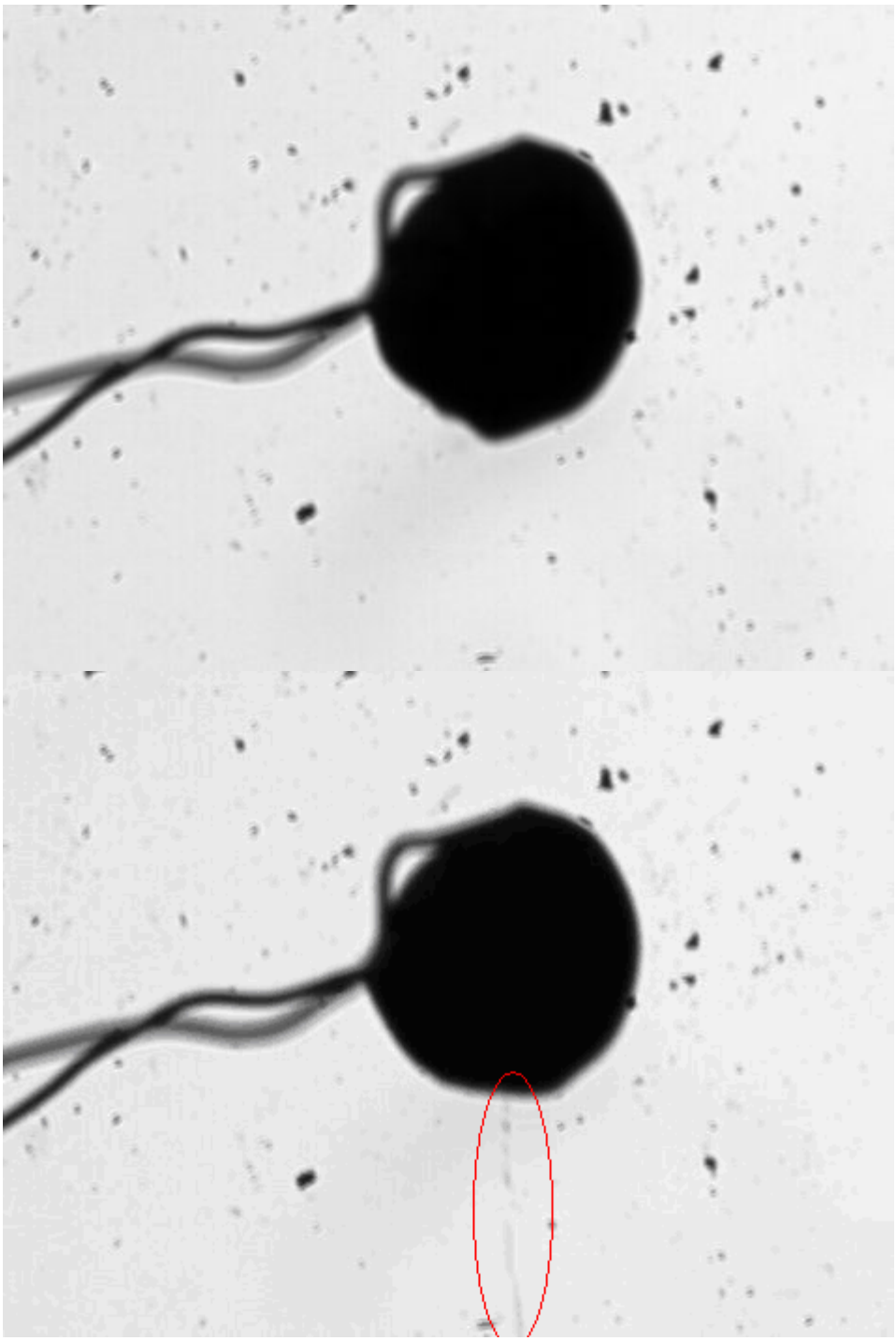

Figure 3-1: Stream Breakup Sequence (D_o=1.67mm, MSAR-30% H2O, 1808 fps)

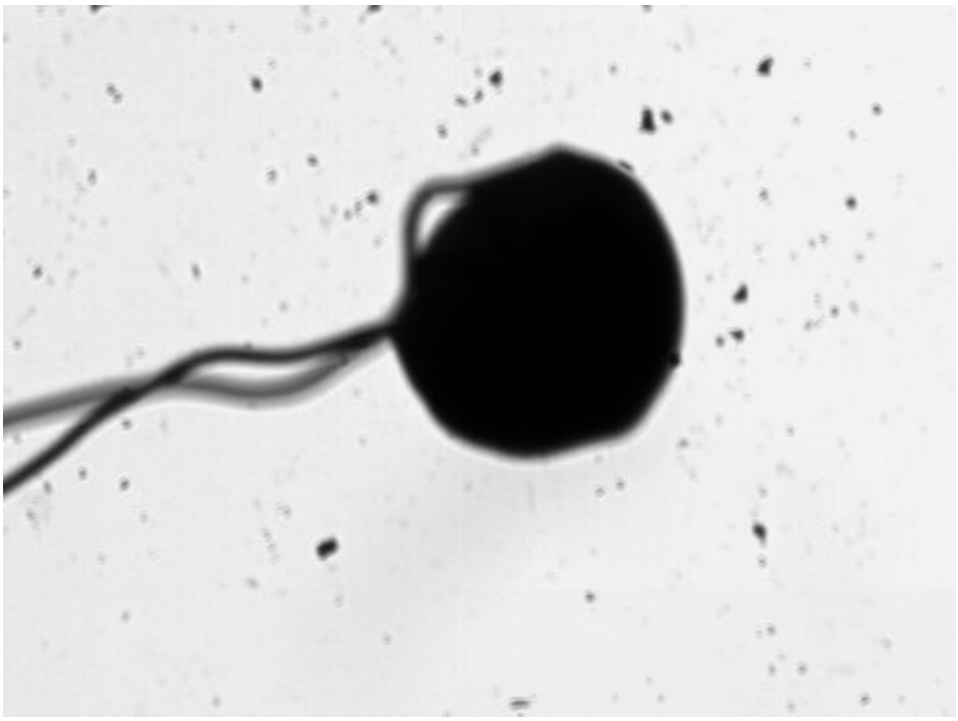

Figure 3-1 Continued

This is the least violent of the three breakups and results in the least amount of matter being separated/released from the parent droplet. It is postulated that there is just enough nucleation energy to pierce the viscous shell of the parent droplet releasing internal matter just as a needle may pierce the skin. The mass that is released depending on its velocity will be released either as a stream or sphere/droplet. At high velocities the stream breakup mass will be released as a stream, whereas at low velocities as a droplet. If enough time elapses without ignition of the released matter, the deceleration of streams will eventually result in them obtaining their lowest energy form: a sphere. This is also true of the two other breakup regimes. In summary, in a stream breakup the matter essentially expels from the surface of the parent droplet with little to no rupturing of the viscous oil shell.

Localized breakups are distinguished by a localized area on the surface of the parent droplet becoming compromised, i.e., the viscous outer layer becoming discontinuous and the subsequent expelling of satellite droplets and matter from the interior of the parent through this break in the outer shell. Figure 3-2 depicts a localized breakup sequence.

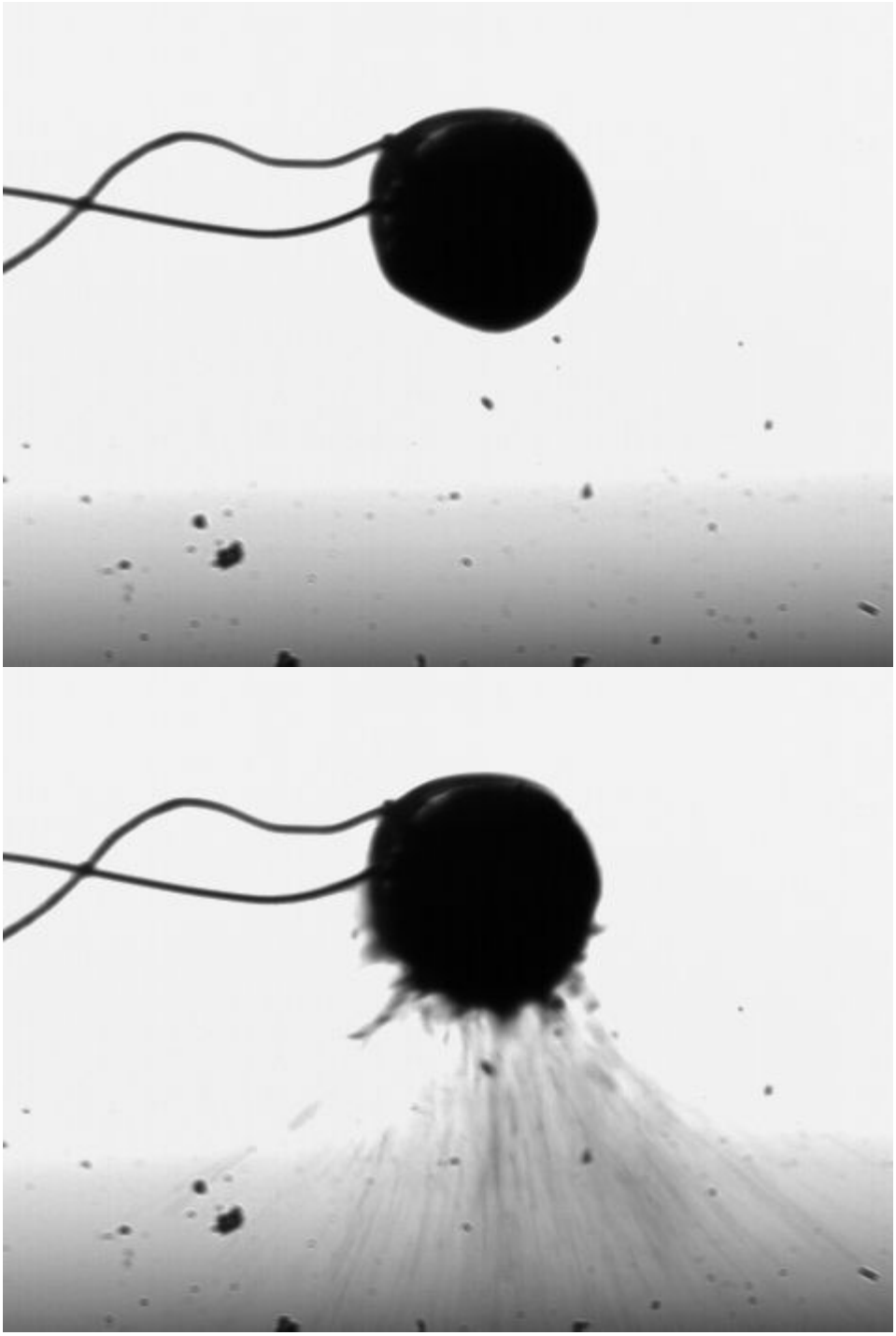

Figure 3-2: Localized Breakup Sequence (D_o= 1.51 mm, MSAR HFO/PPA, 1808 fps)

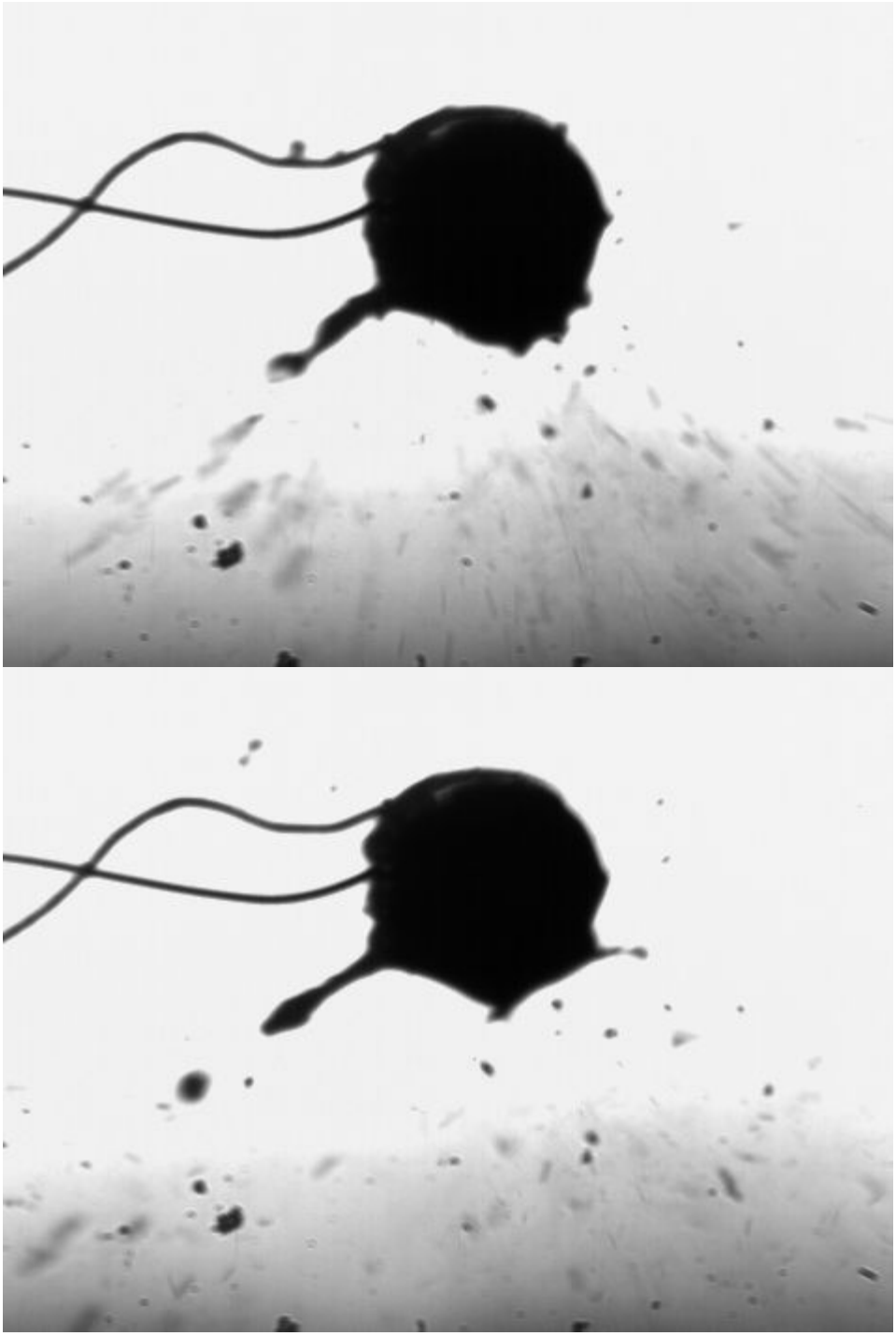

Figure 3-2 Continued

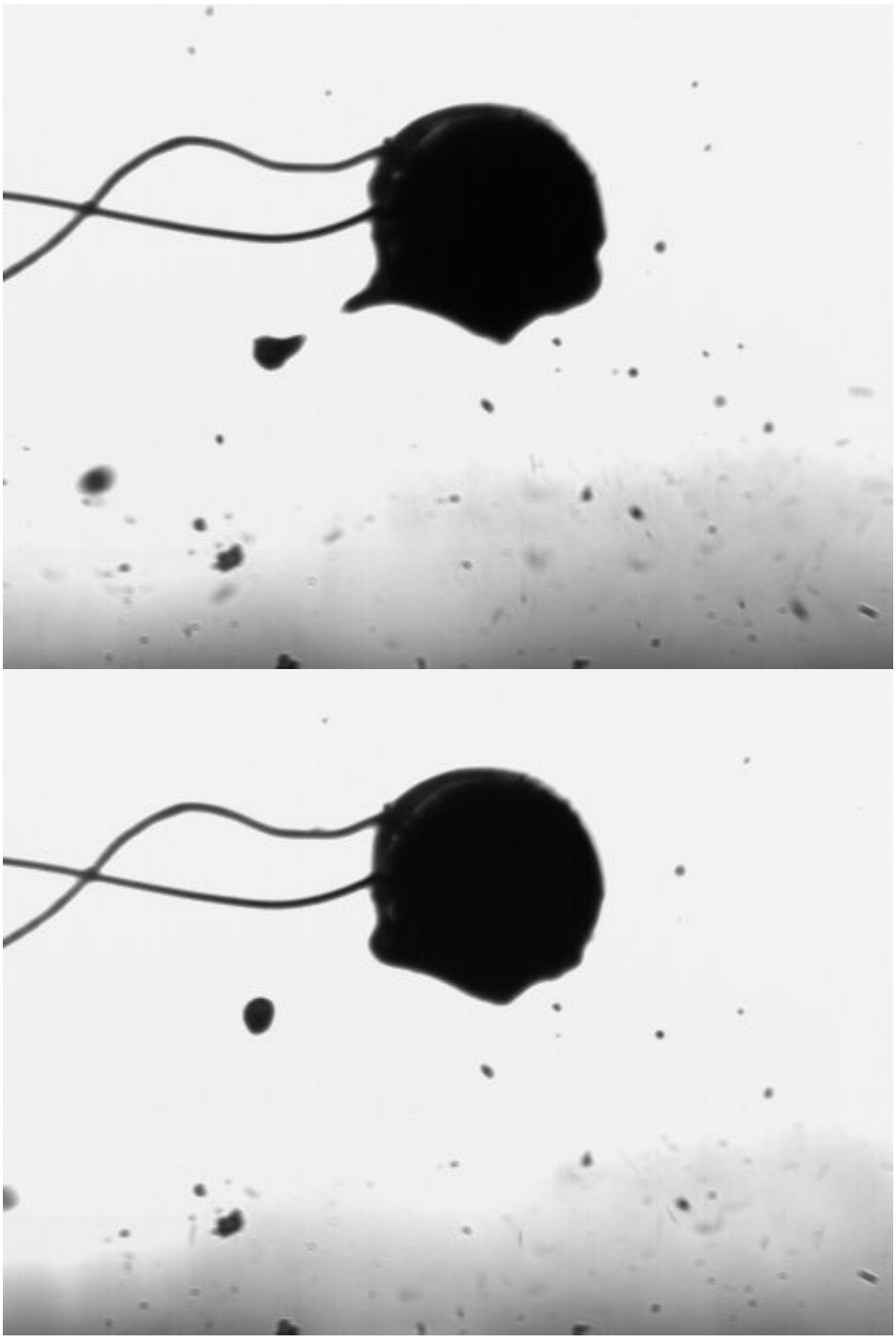

Figure 3-2 Continued

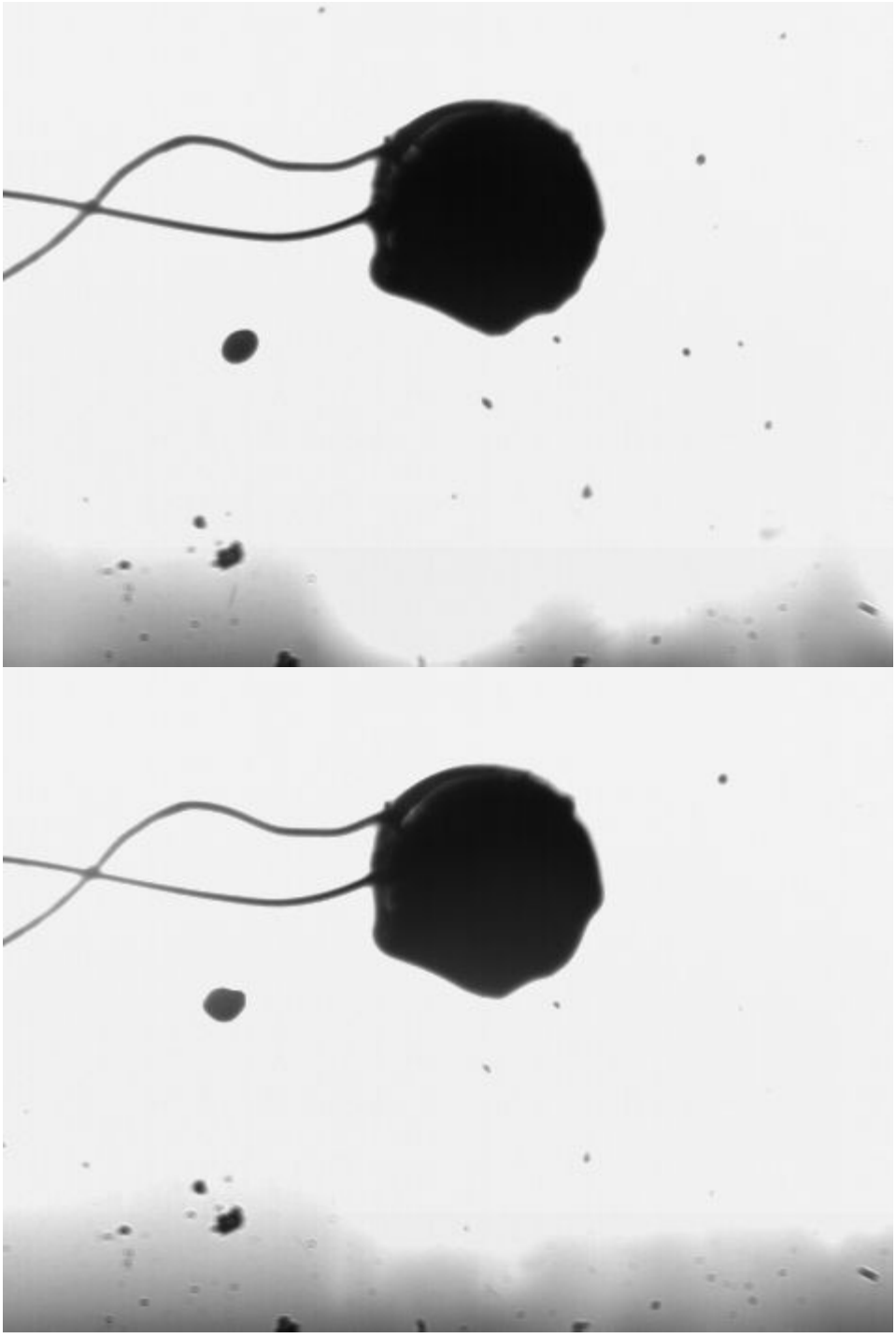

Figure 3-2 Continued

The end of a localized breakup is marked by the recovery of the parent droplet, i.e., the reestablishment of continuity of the oil shell by means of surface tension. The outer shell

fractures open into ligaments and tentacle like structures in a localized breakup giving way to the release of internal matter. Often there is enough force from the breakup to also release portions of the outer shell from the parent droplet along with the internal matter.

The third and final breakup regime, the large violent breakup, is distinguished by the compromising of half or more of the droplet surface in the breakup and the complete distortion of the droplets spherical geometry. A large violent breakup releases more matter than a stream or localized breakup and sometimes results in the complete annihilation of the parent droplet into smaller satellite droplets and masses. A large violent breakup occurs in three steps. The first step is distinguished by the release of high velocity streams from a point on the parent droplets surface similar to a stream breakup, but at much higher velocity and volume. The streams look like a radial display of needles or a spray with its origin being a point on the parent droplets surface. The second step is the splitting or rupturing open of the outer shell propagating from the stream release point. The third and final step is the recovery of the parent droplet distinguished by the reformation of the parent droplets spherically geometry and outer viscous shell. Figure 3-3 displays a large-violent breakup sequence.

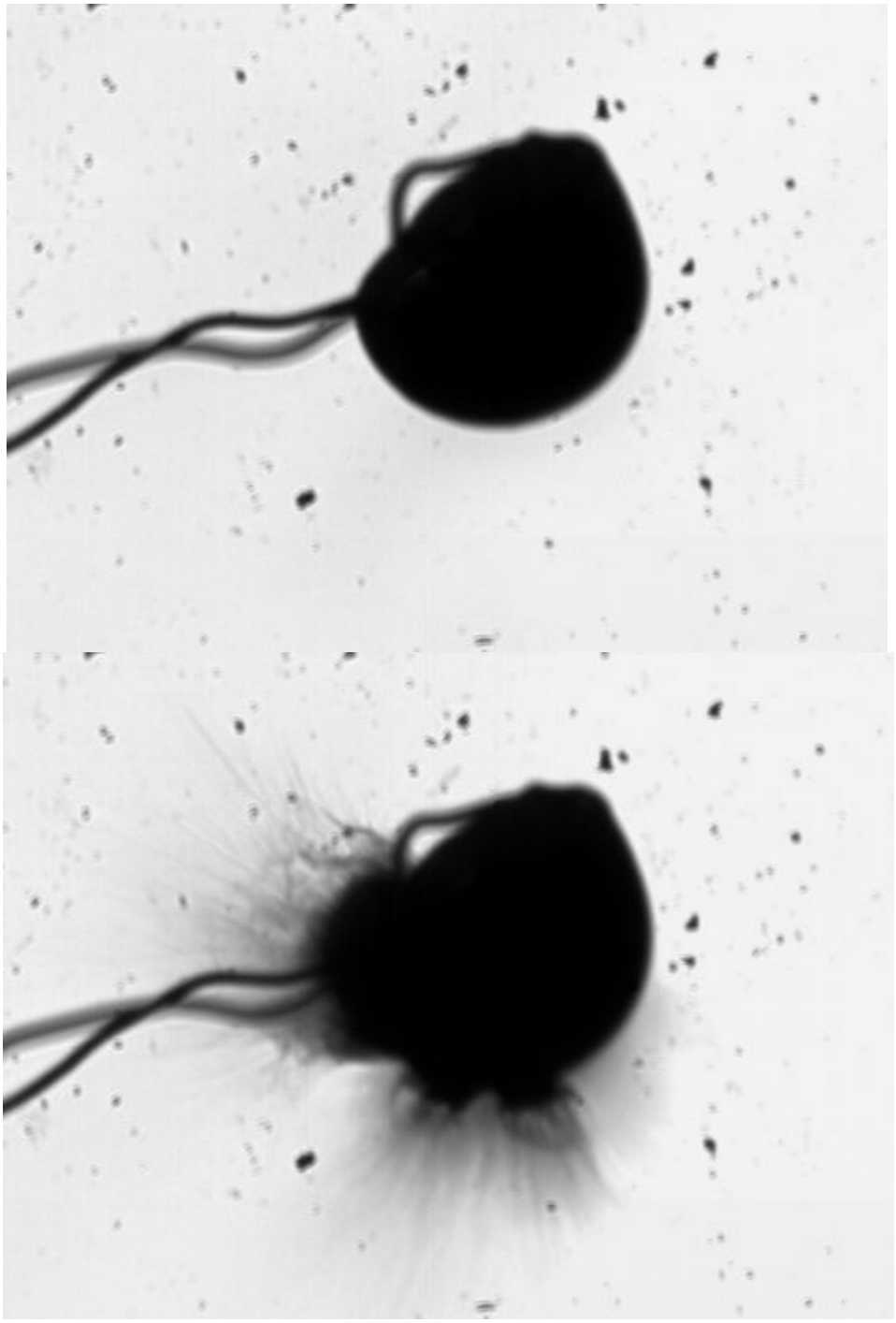

Figure 3-3: Large-Violent Breakup Sequence (D_o=1.67mm, MSAR-30% H2O, 1808 fps)

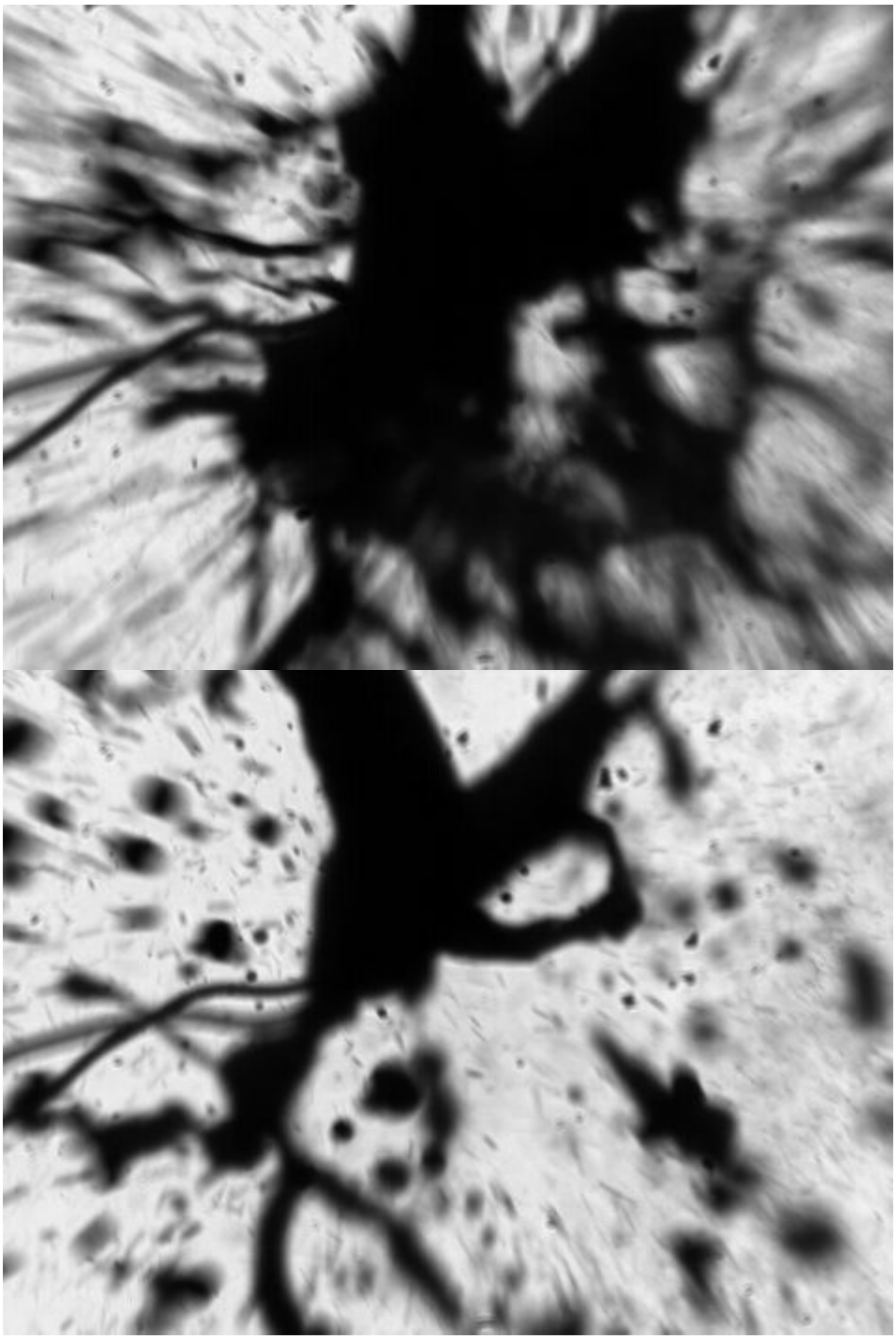

Figure 3-3 Continued

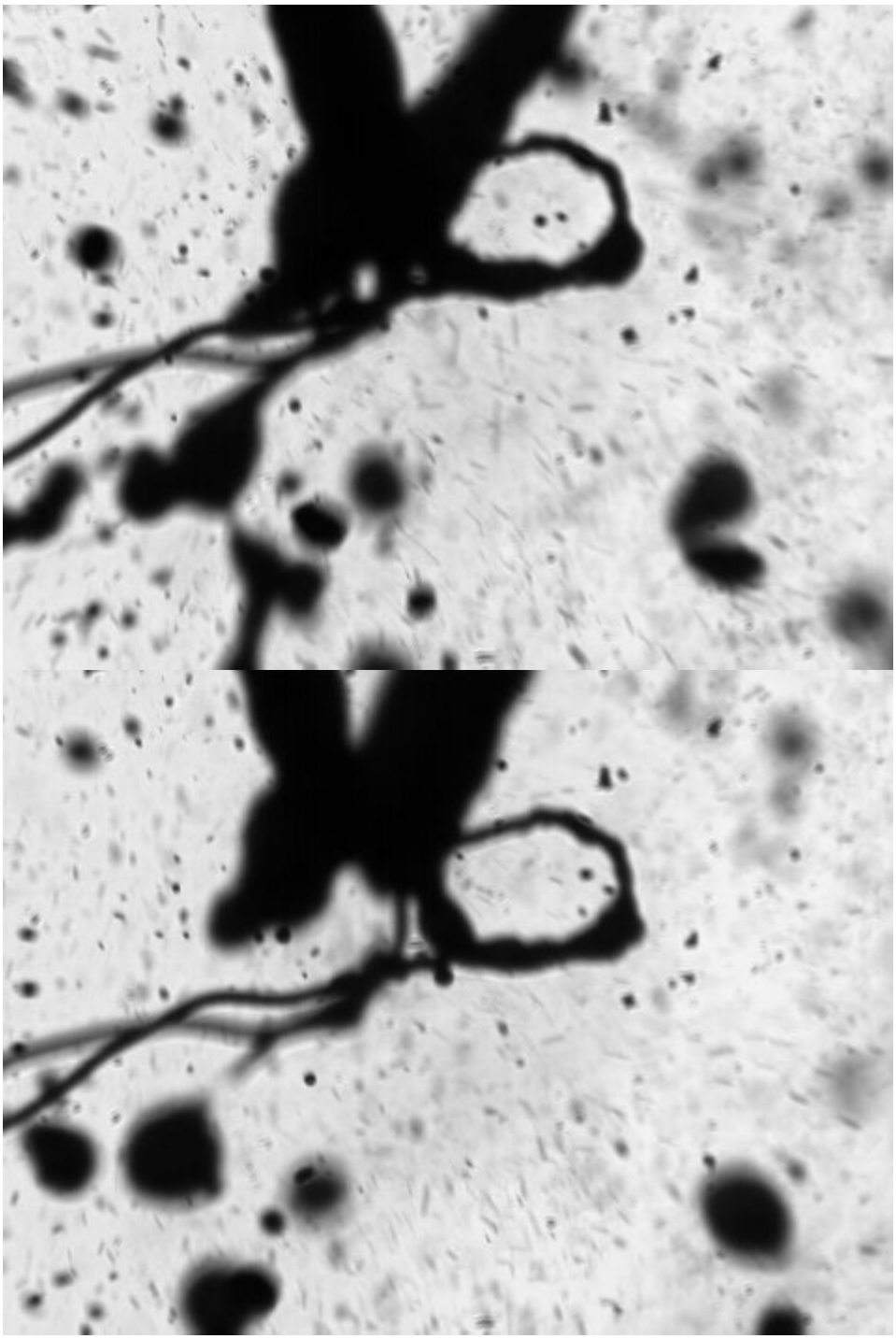

Figure 3-3 Continued

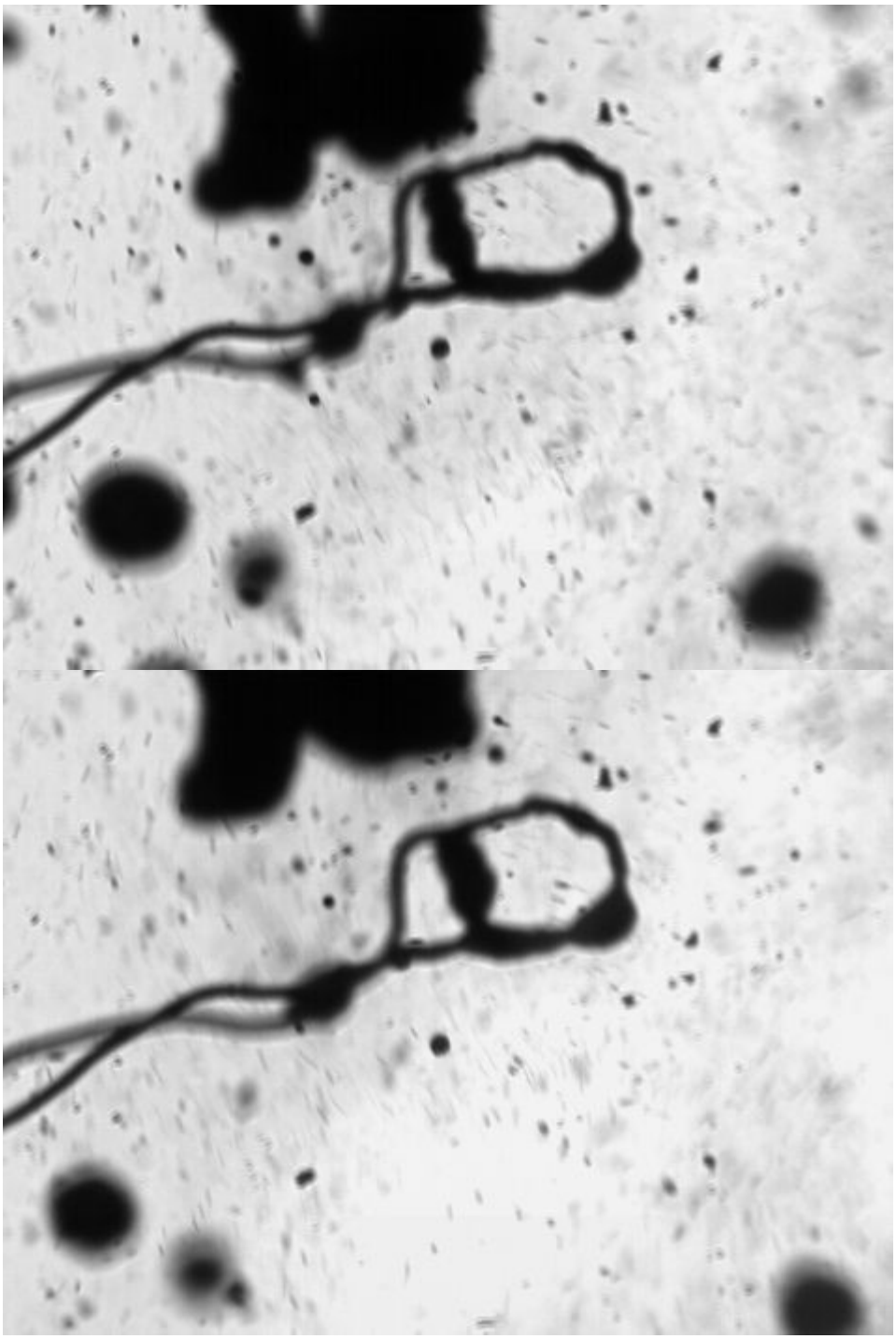

Figure 3-3 Continued

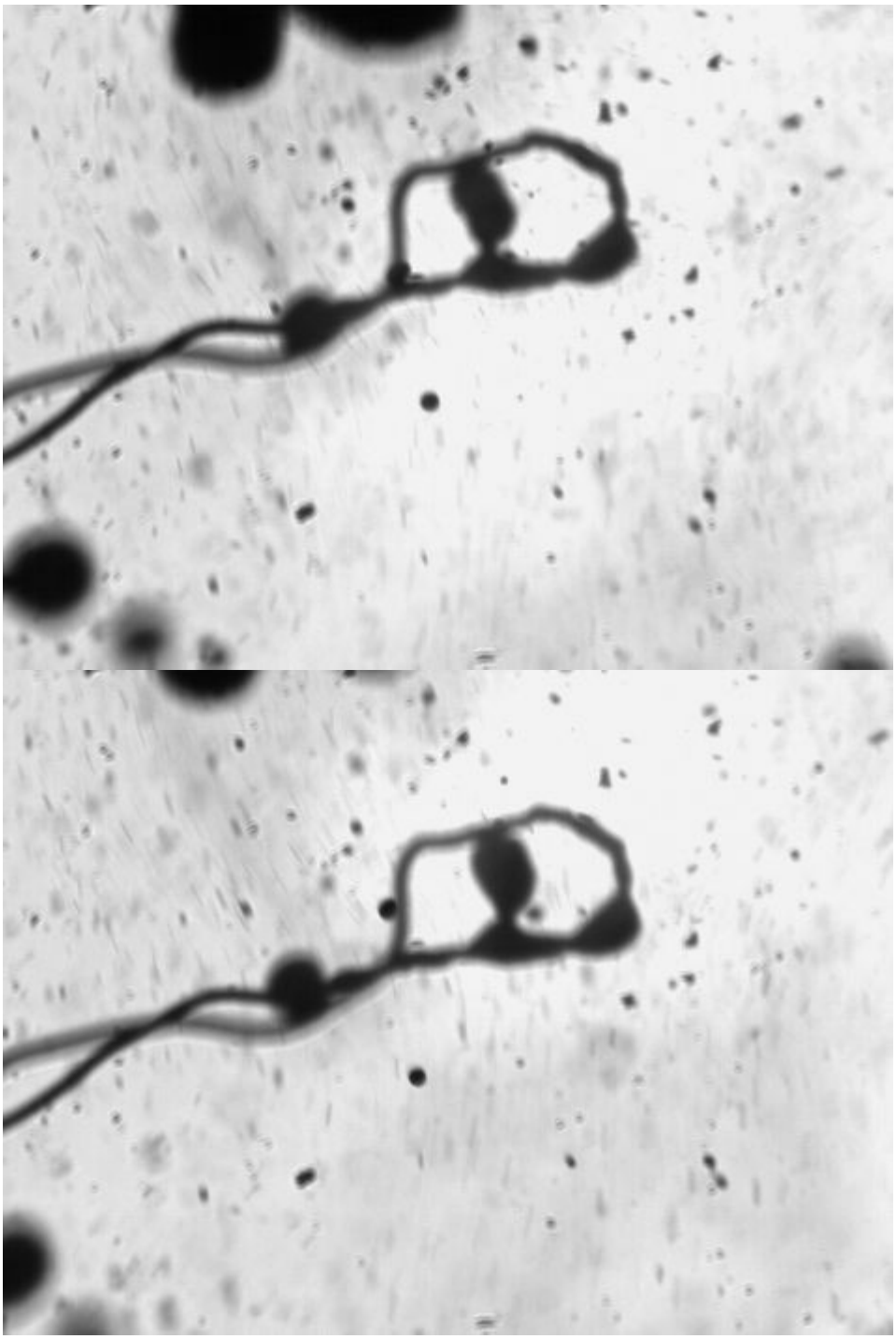

Figure 3-3 Continued

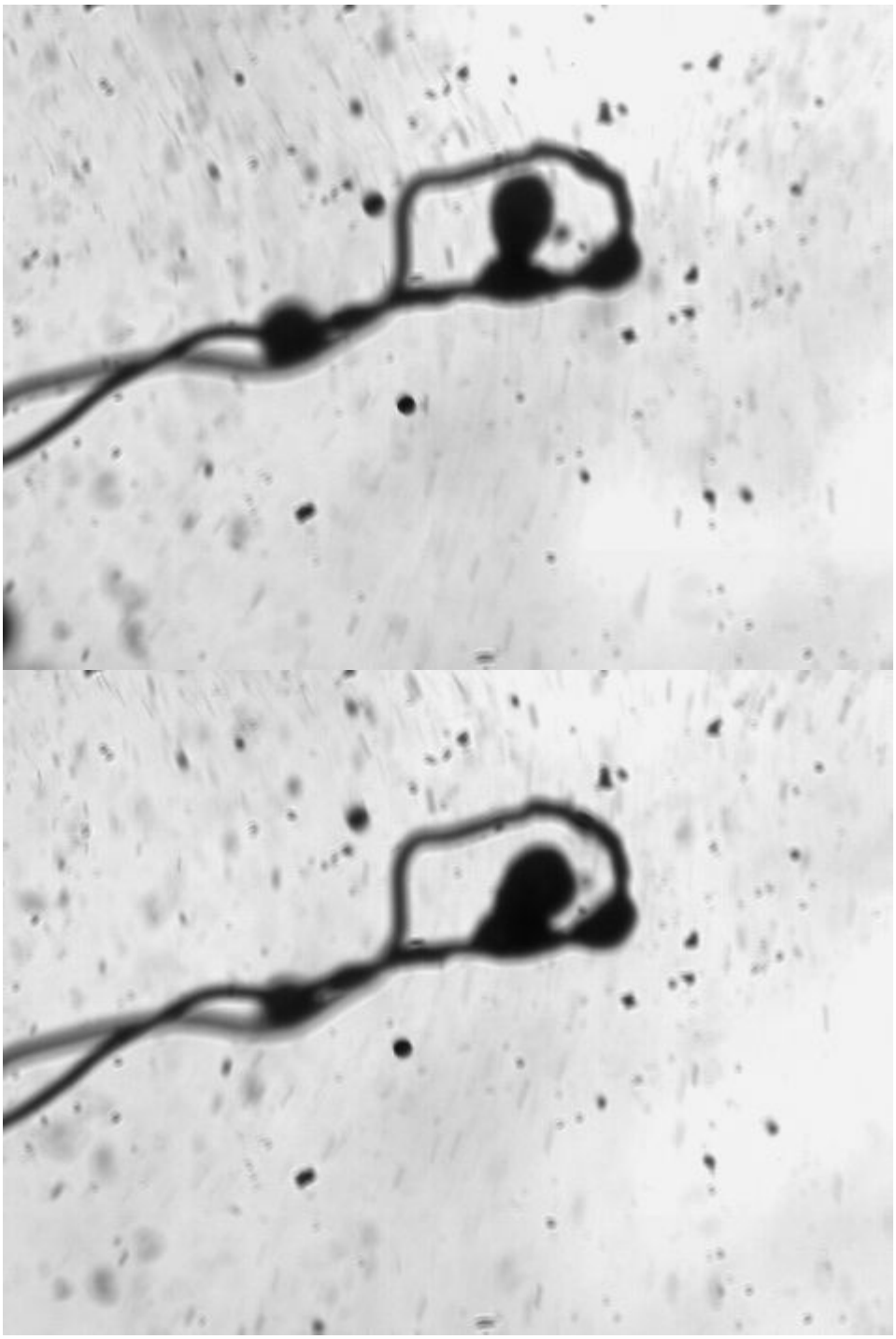

Figure 3-3 Continued

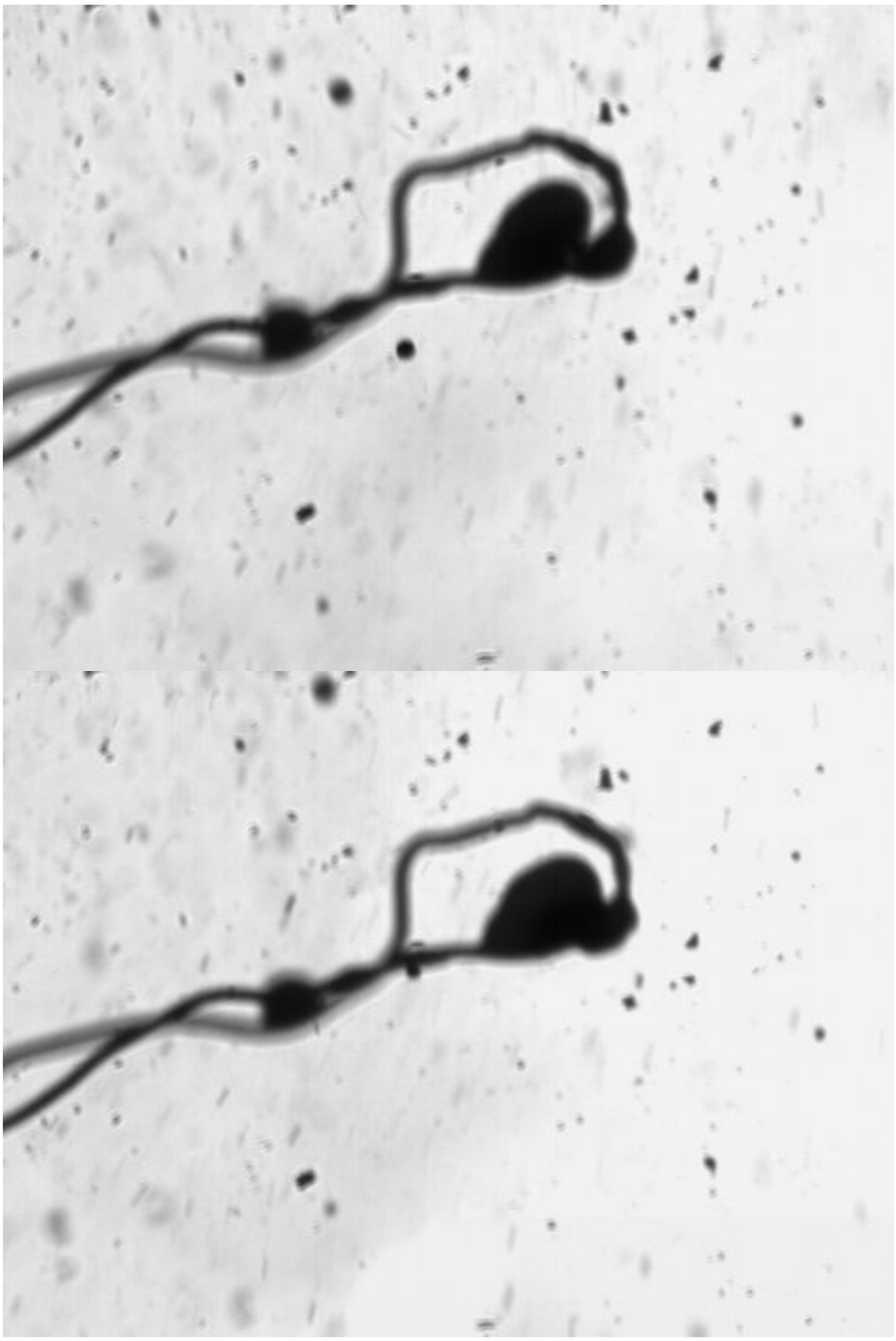

Figure 3-3 Continued

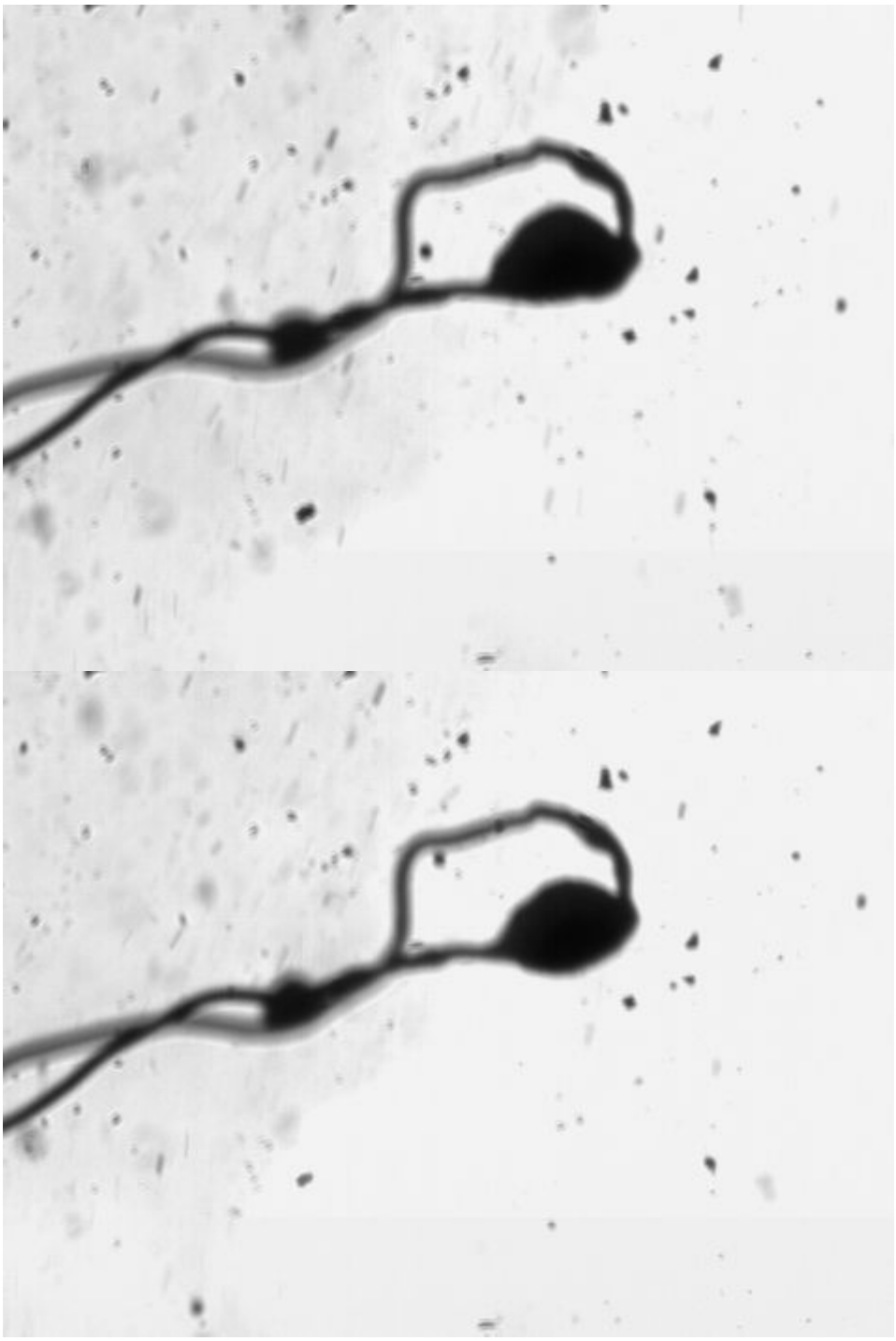

Figure 3-3 Continued

None of the three breakup regimes appear to originate from the center of the droplet, which does not support Zeng and Lee's (2007) model of a single nucleation

bubble originating at the droplets center. Other emulsified fuels could potentially follow this model, but MSAR certainly does not. A free-falling non-convective environment could also potentially produce the desire results Zeng and Lee are looking for in their model. This author postulates that the localized nature of the micro-explosiveness of the observed MSAR droplet is a result of Hill's spherical vortices within the interior of the droplet. Nucleation cannot be assumed to be uniform throughout the parent droplet's volume. These vortices result in unsteady non-radial heating of the MSAR droplets resulting in the formation of nucleation chambers or pockets within the interior of the droplet. Also the author does not want to rule out the possibility of the formation of fuel shells within the fuel shell that could promote the assumption that micro-explosive pockets are present, i.e., coalescence of fuel surrounding water may not be limited to the surface fuel shell. Even the most intense of the large violent breakup that will annihilate the parent droplet will not stem from the center of the droplet, but will begin from a point nearer to the surface and propagate its energy to the rest of the droplet.

There is a fourth regime of activity at the parent droplet surface, but is not categorized as a breakup. The fourth regime is surface bubble nucleation growth. Vapor bubbles may form within the interior of the droplet causing the parent droplet and the viscous outer shell to bulge. Just as in a breakup this bulging may be localized greatly distorting the parent droplet's spherical geometry. There are two scenarios that mark this fourth regime. The first is the formation and collapse of the vapor bubble, and the second is the dissipation of the vapor bubble to the droplets surface and subsequent popping of the bubble releasing the vapors contained within it to the environment. The second mode may or may not result in the ignition of the released vapor. It is postulated that ignition is

dependent on the composition of the vapor, i.e., percent water content, exiting from the nucleation bubble and the surrounding temperature. The fourth regime is believed to occur when there is one or a combination of the following: a lack of nucleation energy present to cause regimes one through three to occur, the fuel shell has not yet formed or the fuel shell is recovering from a previous breakup. The MSAR droplets appear to cycle between these four regimes throughout the burning of the MSAR droplet.

3.2 The Burning of an MSAR Droplet

Like the combustion of non-emulsified fuel droplets the start of the MSAR combustion process is marked by a heating period. During this heating period the MSAR droplet will experience surface rippling due to the convective flow surrounding it as a consequence of the methane diffusion flame. The surface rippling will give way to internal circulation and an increased rate of heat transfer to the droplet center. The internal circulation is presumed to assist fuel shell formation by promoting the coalescence of bitumen at the surface. Bubble nucleation (regime four) dissipating towards the surface of the droplet will also begin during this period and it assumed that this initial nucleation bubbles are essentially purely that of water vapor because there is no ignition of the vapors. This stage is thought to assist in removing water from the surface of the parent droplet further promoting the formation of the fuel shell. Given this, the heating period is also marked by the formation of the fuel shell. Eventually, the release of vapors due to nucleation at the surface will cease or slow, and the parent droplet will begin to bulge as a result of the nucleation. The ceasing of bubble nucleation and water vaporization at the surface marks the formation of the fuel shell. The heating period may or may not culminate with the ignition of the parent droplet itself and the

forming of an enveloping diffusion flame surrounding the droplet, however if the enveloping flame forms it will most always distinguish with occurrence of any of the three breakup regimes or will never propagate for more than approximately 5.00 milliseconds. Interestingly enough, throughout the burning process enveloping diffusion flames may intermittingly form around the parent droplet but the visible flame will most often be present no longer than the specified 5.00 milliseconds. It is postulated that there must be short periods in which normal droplet regression occurs at the MSAR droplet surface to provide fuel vapor for these intermittent enveloping flames to form. The fuel shell (assumed to be made up of the least volatile components of the MSAR droplet) and the consumption of oxygen by pre-vaporized, i.e., superheated matter exiting during breakups are thought to be the reasons for the difficulty for an enveloping diffusion flame to consistently propagate around the MSAR droplet. A third postulation is that the force of micro-explosions causes a quenching of the surrounding atmosphere of oxygen not allowing a diffusion flame to be sustained and micro-explosions also release the lower temperature interior gases of the droplet decreasing, extremely briefly, the ambient temperature surrounding the parent droplet.

The second stage in the combustion process of the MASR fuel droplet is the initiation of the breakup regimes normally beginning with the stream breakup. During this stage the dynamism of the parent droplet due to trapped internal nucleation energy is much more prevalent sometimes causing large bulges or the appearance of rippling at the droplet surface. It is of importance to note that most of the initial breakups originate at the thermocouple-parent droplet interface, however breakup origination is not limited to this criteria. Heterogeneous nucleation, as would be expected, is thus evidenced to occur

at lower temperatures than homogeneous nucleation for the MSAR droplets, and it is this heterogeneous nucleation that most often leads to the first set of breakups. With increases in temperature of the parent droplet homogeneous nucleation will begin and breakups will occur at all interfaces within the MSAR droplet.

With this second stage the MSAR droplet begins a cycle consisting of bubble nucleation growth (regime four), stream breakups (regime one), localized breakups (regime two), large violent breakups (regime three), and finally droplet recovery and fuel shell reformation. Fuel shell reformations are also present after regimes one and two but the recovery is much faster than for regime three breakups. Each breakup in the cycle is also marked by the ignition and flame propagation of released vapor and satellite droplets. There are also second generation breakups, i.e., breakups of satellite droplets, which are also marked by a period of ignition and flame propagation. The subsequent section will discuss in more detail the path, ignition, and burning of satellite droplets. This cyclic process is very rapid and without the ability of a frame by frame analysis the combustion in real time appears as a continuous disruptive burning process.

The third and final stage in the burning of an MSAR droplet is a final large-violent breakup that results in the complete vaporization and combustion of the parent droplet leaving no liquid mass behind for a reformation process and the beginning of another burning cycle. Unlike heavy fuel oils the burning of an MSAR droplet does not culminate with a coke combustion stage and consequently leaves no visible carbonaceous residue behind, a great advantage to say the least. Many of the experimental runs did not culminate with this occurrence, however, because often times the droplet would be heated to the point at which it would loose surface tension with the thermocouple junction and

fall or the force of a breakup would cause the release of the droplet from the thermocouple. However, this occurrence, although undesirable for retrieval of droplet core temperature data, was not without positive consequences. The burning of the falling droplet was able to be captured by the lengthwise frame of the CASIO high-speed camera. First and foremost these observations proved that micro-explosion of the MSAR fuel is not limited to heterogeneous nucleation. Secondly, the empirical observations showed that the micro-explosive rate of the falling droplet was increased compared to the droplet being stationary within the convective stream. Thirdly, the waiting period for large-violent breakups to occur within the burning cycle was greatly decreased. Theory would point to these observations being a consequence of an enlarged convective coefficient, increased conduction within the droplet interior, and an increase in magnitude of the Weber number. Complementing this increase in heat transfer could also be an increase in fuel shell reformation rate.

3.3 Satellite Droplets and Maximum Breakup Velocities

Satellite droplets are those droplets released from the parent droplet as a result of micro-explosion. There are two types of satellite droplets: 1) Those that shoot out from the interior of the parent droplet due to a breakup and 2) those that form from ligaments that breakaway from the fuel shell as the result of a breakup. Overcoming surface tension plays a large role in determining whether the second type of satellite droplet will form, and thus is dependent on the intensity of the breakup. It should be noted that as determined in previous work, the intensity of micro-explosion is shown to be highly dependent on the size of the parent droplet with larger droplets having more intense breakups and thicker fuel shells. The path of a satellite droplet is initially dominated by

the momentum dissipated to it from the force of the micro-explosion, but after a short time period the satellite droplets path becomes dominated by the convective flow of the surrounding methane diffusion flame. During the momentum transfer from breakup momentum to flame momentum the satellite droplets take a parabolic like path until they are fully incorporated into the upward flow of the flame.

The majority of satellite droplets ignite almost instantly upon their release, but the larger satellite droplets may travel for a distance before ignition. At the normalized height of 108 the visible methane flame is not always present at the parent droplet interface, and during these intermittent periods there will be continuous satellite droplet release without ignition until the satellite droplets come in contact with the visible flame. However, relatively large satellite droplets maybe released from a parent droplet at the normalized height of 50 as well, but it is less frequent because of the continuous presence of the heat source. Some satellite droplets will travel the length of the frame without ignition: a distance of approximately 95.00 mm. The burning of a satellite droplet is greatly dependent on satellite droplet concentration. Just as in spray combustion, the micro-explosion of droplets requires knowledge of three distinct areas: 1) the burning mechanism of individual droplets, 2) the statistical methods for describing groups of particles and 3) the manner in which the behavior of these groups modify the behavior of the gas in flow systems (Kuo, 1986). (From this one can see the complexities in trying to optimize the burning of micro-explosive fuels. See Kuo, 1986 for details on statistical methods for describing groups of droplets in a multi-phase flow). Areas of high satellite droplet density will not burn individually in liquid-vapor diffusion flames, but rather will burn in a cloud that is almost identical to a gaseous diffusion flame. This cloud will

propagate radially in the wrinkled laminar flame regime until convective flow takes over and the cloud begins to stretch lengthwise. Figure 3-4 below shows snapshots that are rotated horizontally of one of these sequences.

Figure 3-4: Micro-Explosion – High Density Satellite Droplet Concentration Regions Result in Gaseous Cloud like Burning and Low Density Regions Result in Enveloping Flame Burning (D_o=1.67 mm, MSAR 30% H2O, 1200 fps)

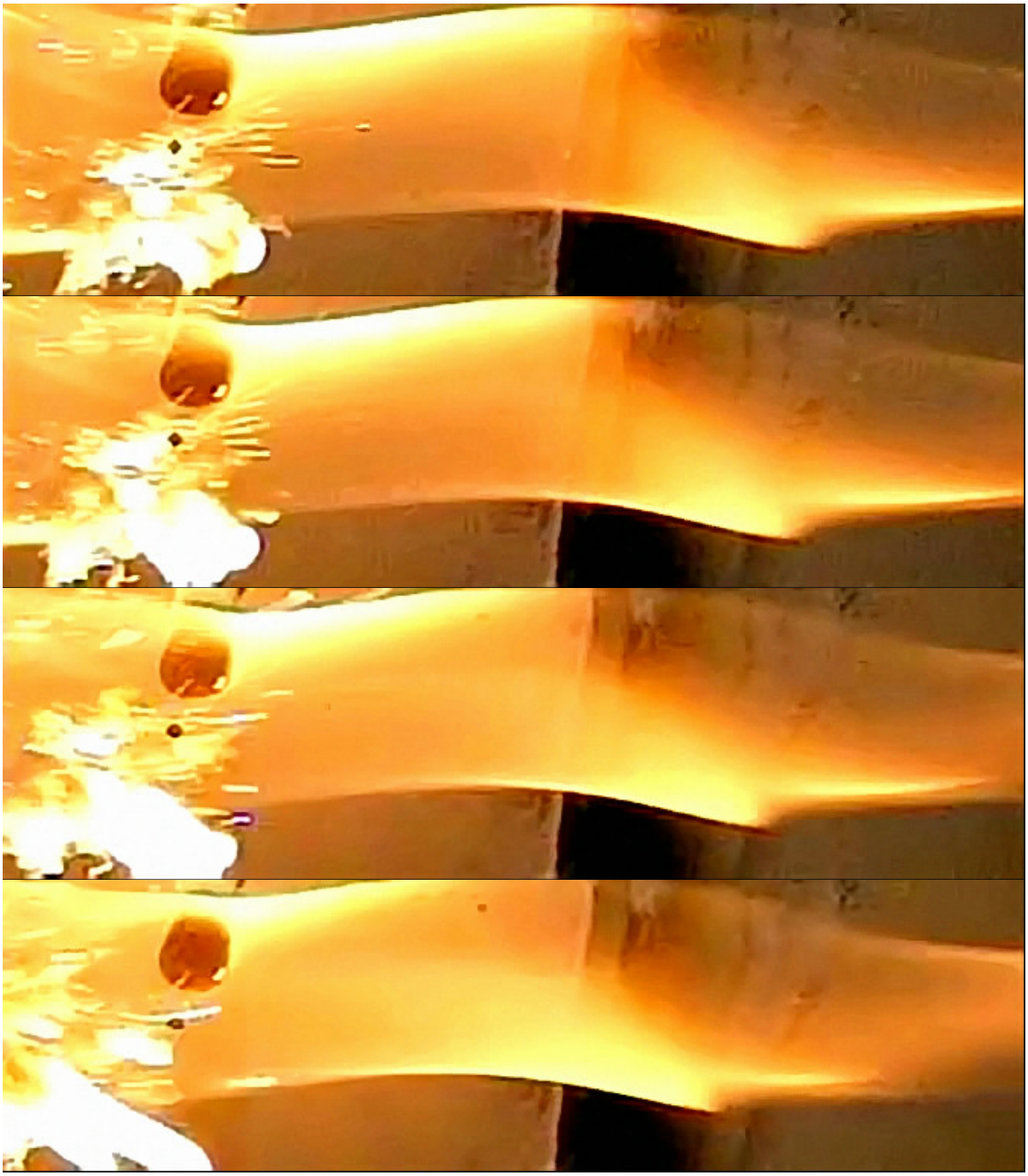

Figure 3-4 Continued

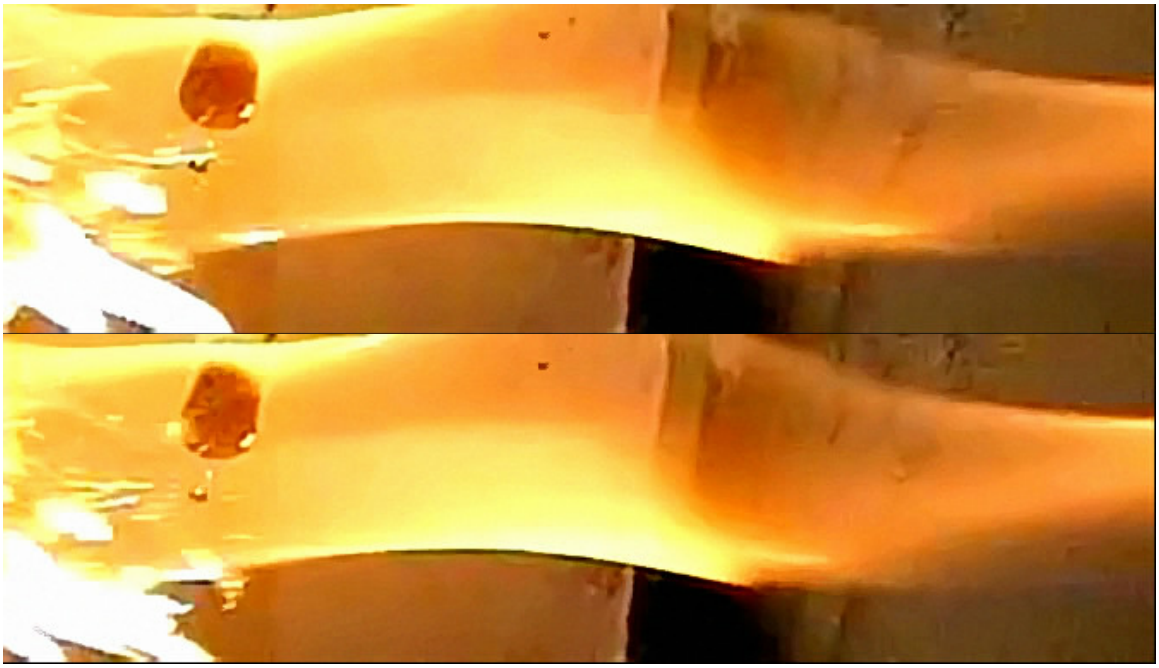

Figure 3-4 Continued

In areas of low satellite droplet concentration, a satellite droplet will burn individually with an enveloping diffusion flame. The enveloping diffusion flames frequently burn with a blue tint, while the gaseous clouds burn with a yellow-white flame. Figure 3-4 also shows individual satellite droplets burning with an enveloping diffusion flames. The methane diffusion flame burns orange relative to the bitumen fuel.

Qualitative evidence from the high-speed videos shows that second generation micro-explosion can occur in MSAR satellite droplets with diameters less than 100 microns. Theoretically this makes sense because the micro-dispersed bitumen droplets in MSAR are on average between 3-5 microns.

Because of the disruptive nature of micro-explosive fuels it is extremely difficult to define trends and present the data; so much of what is occurring is statistically random. Unlike atomization studies not even constant nozzle diameter (parent droplet “blow holes”), flow rate (flow of satellite material), or local homogeneous flow (LHF) can be

controlled or assumed. Consequently, previous work has mainly consisted of qualitative evidence with some statistical analysis. The reader should keep this disclaimer in mind as the quantitative data is presented. Additionally, quantitative data in this study is limited by the instrumentation used and the methods used to analyze the data as a result of the instrumentation. Studying multiphase turbulent flows is not only a difficult but expensive undertaking.

The velocities of satellite droplets released from the parent droplet vary for each type of breakup regime. The maximum breakup ("micro-explosive") velocity is defined as the distance of the farthest mass/satellite droplet expelled from the parent droplet -- resultant from a micro-explosion -- divided by the number of frames times one over the framing rate. Equation 3 below gives the formulation for maximum breakup velocity

$$V_{max} = \frac{L}{n*\frac{1}{f}} \tag{3}$$

where L is the maximum distance a satellite droplet traveled in n frames and f is the framing rate in hertz. The number of frames (n) is one unless specified otherwise. Tables 3-1 through 3-5 list the average maximum breakup velocity, maximum breakup velocity, and minimum breakup velocity within the maximum breakup velocity range for the three breakup regimes for selected experimental runs of the MSAR fuels. Table 3-1 gives these results for the MSAR – 70% hydrocarbon fuel at the normalized height of 50, while Table 3-2 gives these results for the fuel at the normalized height of 108. Similarly, Table 3-3 gives these results for the MSAR PPA/HFO fuel at the normalized height of 50, while Table 3-4 gives the results for the fuel at the normalized height of 108. Velocity data was only obtained at the normalized height of 50 for the MSAR –

80% hydrocarbon fuel and its results for selected experimental runs are listed in Table 3-5.

Table 3-1: MSAR – 70% Hydrocarbon (normalized height of 50) maximum breakup Velocity data

Fuel	MSAR-70% Hydrocarbon								
Test #	MSAR 70-50 026-II			MSAR 70-50 026-III			MSAR 70-50 026-VI		
Breakup Type	Large	Local	Stream	Large	Local	Stream	Large	Local	Stream
Maximum Velocity (m/s)	17.08	9.64	15.01	16.76	12.25	16.21	19.52	8.74	15.23
Minimum Velocity (m/s)	5.21	2.25	1.69	9.42	2.91	2.09	5.67	3.22	1.91
Avg. Maximum Velocity (m/s)	10.26	5.26	5.08	13.19	5.87	7.49	9.09	6.44	5.65

Table 3-2: MSAR – 70% Hydrocarbon (normalized height of 108) maximum breakup Velocity data

Fuel	MSAR-70% Hydrocarbon								
Test #	MSAR 70-108 024-I			MSAR 70-108 025-I			MSAR 70-108 025-III		
Breakup Type	Large	Local	Stream	Large	Local	Stream	Large	Local	Stream
Maximum Velocity (m/s)	15.50	5.82	11.26	24.79	7.15	13.71	24.33	12.05	9.98
Minimum Velocity (m/s)	15.50	4.01	4.29	6.9	5.9	3.76	7.04	5.76	4.14
Avg. Maximum Velocity (m/s)	15.50	4.97	6.72	12.23	6.38	7.22	11.46	8.92	6.58

Table 3-3: MSAR – PPA/HFO (normalized height of 50) maximum breakup Velocity data

Fuel	MSAR-PPA/HFO								
Test #	MSAR PPA-50 026-I			MSAR PPA-50 026-III			MSAR PPA-50 027-II		
Breakup Type	Large	Local	Stream	Large	Local	Stream	Large	Local	Stream
Maximum Velocity (m/s)	16.28	11.05	13.5	11.45	10.18	8.14	16.67	8.58	7.07
Minimum Velocity (m/s)	9.64	1.69	2.68	6.52	1.88	1.21	11.27	3.09	0.922
Avg. Maximum Velocity (m/s)	12.96	6.26	6.12	8.95	5.13	4.71	14.12	4.91	4.09

Table 3-4: MSAR – PPA/HFO (normalized height of 108) maximum breakup Velocity data

Fuel	MSAR-PPA/HFO								
Test #	MSAR PPA-108 022-III			MSAR PPA-108 024-II			MSAR PPA-108 024-III		
Breakup Type	Large	Local	Stream	Large	Local	Stream	Large	Local	Stream
Maximum Velocity (m/s)	14.15	14.3	10.34	15.50	10.45	14.32	21.22	12.05	14.21
Minimum Velocity (m/s)	7.66	3.25	3.12	8.08	4.32	2.00	7.15	3.53	3.09
Avg. Maximum Velocity (m/s)	9.95	8.74	5.77	10.69	6.58	7.52	14.19	7.77	7.14

Table 3-5: MSAR - 80% Hydrocarbon (normalized height of 50) maximum breakup Velocity data

Fuel	MSAR-80% Hydrocarbon								
Test #	MSAR 80-50 026-I			MSAR 80-50 026-II			MSAR 80-50 027-I		
Breakup Type	Large	Local	Stream	Large	Local	Stream	Large	Local	Stream
Maximum Velocity (m/s)	18.28	15.64	16.92	17.72	14.25	18.07	9.32	8.67	9.54
Minimum Velocity (m/s)	6.20	1.94	1.40	5.83	2.06	0.86	4.06	1.58	1.34
Avg. Maximum Velocity (m/s)	12.29	6.13	6.11	11.54	6.72	5.98	6.26	4.03	5.20

In comparing Tables 3-1 through 3-4 listing the velocity data for MSAR – 70% hydrocarbon fuel and the MSAR – PPA/HFO fuel it is non-conclusive which of the two fuels has greater breakup velocity tendencies. Looking at Table 3-5, however, and comparing it to Tables 3-1 and 3-3 it is apparent that the MSAR – 80% hydrocarbon fuel is associated with breakup velocities that are slower than that of the other two fuels. Generally, the breakup velocities are greater at the normalized height of 108. A more detailed discussion on the consequences of the position of the MSAR fuel droplet within the methane diffusion flame follows.

3.4 Consequences of MSAR's Position within a Methane Diffusion Flame

As aforementioned the MASR droplets were burned within the methane diffusion flame at normalized heights of 50 and 108, respectively. The normalized height of 50 is assumed to be a fuel rich condition, while combustion at the normalized height of 108 was assumed to be a lean condition. These efforts were conducted to quasi simulate the use of MSAR in a spray were droplet size distribution will result in some MSAR droplets vaporizing mid-flame and the heavier ones near the periphery of the flame.

At the normalized height of 50 the average temperature of the methane diffusion flame is approximately 1172 °C. At the normalized height of 108 the flame has an average flame temperature of 850 °C, but a wide range of 458 °C to 1098 °C as a result of flame flapping. The parent droplet temperature time history for experimental run MSAR70-50 026-III (MSAR 70% hydrocarbon, i.e., 30% water, normalized height of 50, Test # 027-III) is shown below:

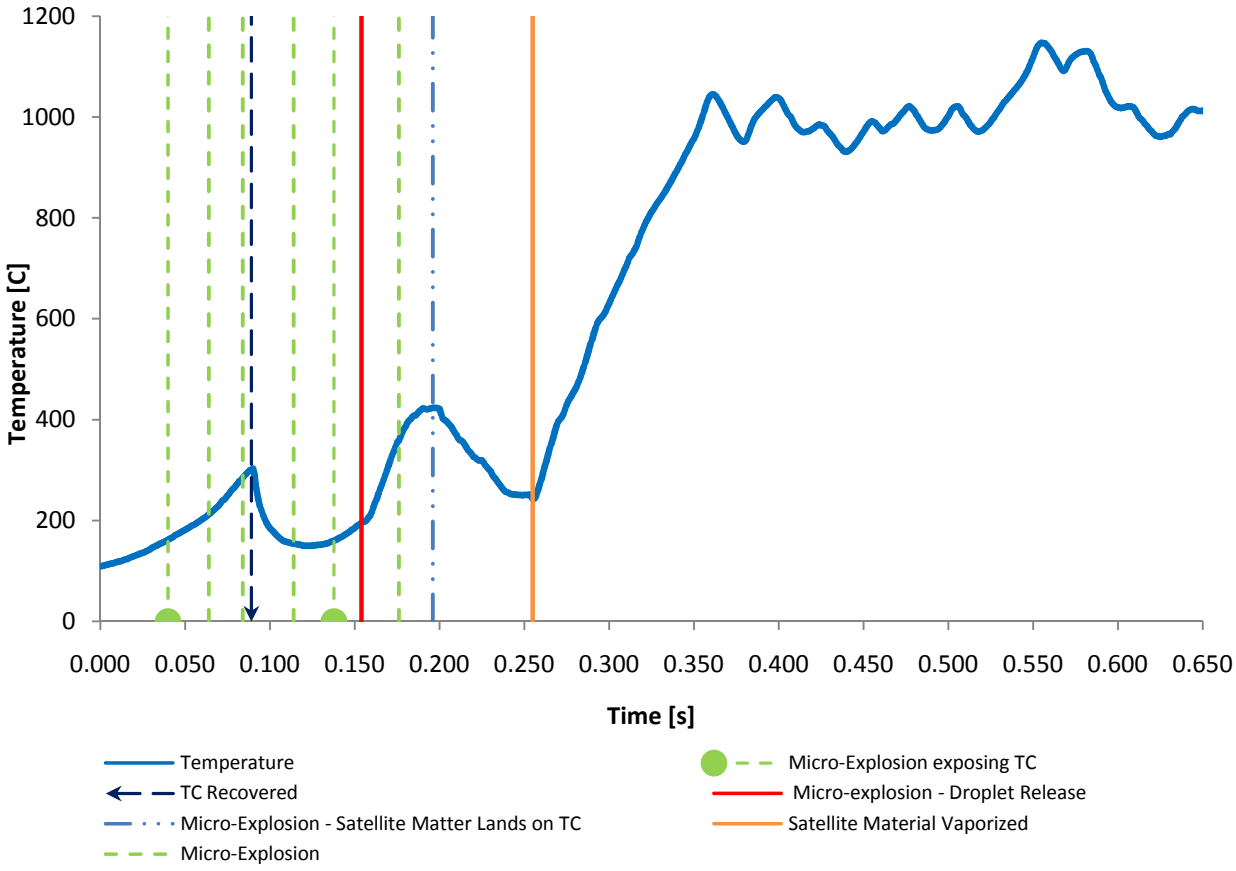

Figure 3-5: Temperature Time History – MSAR70-50 026-III (D_o=1.40mm)

The temperature time history for experiment MASR70-50 026-III is shown here first because it is representative of the entire spectrum of events that can take place during the burning of an MSAR droplet that will adversely affect the temperature data. The following is a descriptive list of those temperature events that will also be used herein to describe the temperature time histories of representative experimental runs. It is important to note that no two experimental runs are identical, but as alluded to earlier they are the victim of such random events as those that follow to describe the temperature data results:

- Micro-Explosion - The occurrences of micro-explosions are indicated by green dashed vertical lines on the temperature time history graphs as seen in Figure 3-4. All micro-explosions indicated on the temperature time history graphs are large-violent breakups. No localized or stream breakups are indicated on the graphs.
- Micro-Explosion Exposing TC Junction – The force of these micro-explosions result in the parent droplet being lifted from the thermocouple junction exposing the TC junction to the methane diffusion flame causing a sharp increase in the temperature gradient. The micro-explosion however does not result in the complete release of the parent droplet from the thermocouple; the parent droplet will still be supported by the thermocouple leads.
- TC Recovered – Occurs when the dynamism of the parent droplet itself causes it to recover the TC junction after having left the junction.
- Micro-Explosion - Satellite Matter Lands on TC Junction – Occurs when the TC junction is exposed, but satellite matter from a micro-explosion of the parent droplet lands on the TC junction surface causing a sharp decrease in the temperature gradient. Event ends with the vaporization of satellite material from the TC junction resulting in a change in the temperature gradient from negative to positive.
- Micro-Explosion – Droplet Releases – The force of a micro-explosion causes the parent droplet to loose tension with the thermocouple and begin free fall. This step is normally followed by a decrease in the temperature

gradient as a result of vaporization of left behind residue and then a sharp increase in temperature because the TC is entirely exposed to the flame.

- Droplet Release – Droplet looses tension with thermocouple and begins a free fall.

As can be seen in Figure 3-5, plots of temperature time histories culminate with the temperature increasing up to the methane flame temperature of the representative height. Figure 3-5 is also representative of the high micro-explosive rate of MSAR burning in general and relative to the normalized height of 50. The micro-explosive rate at normalized height of 50 is much greater than the micro-explosive rate at the normalized height of 108. Figure 3-6 below is a “representative” graph of the temperature time histories of an MSAR droplet burning at the normalized height of 108.

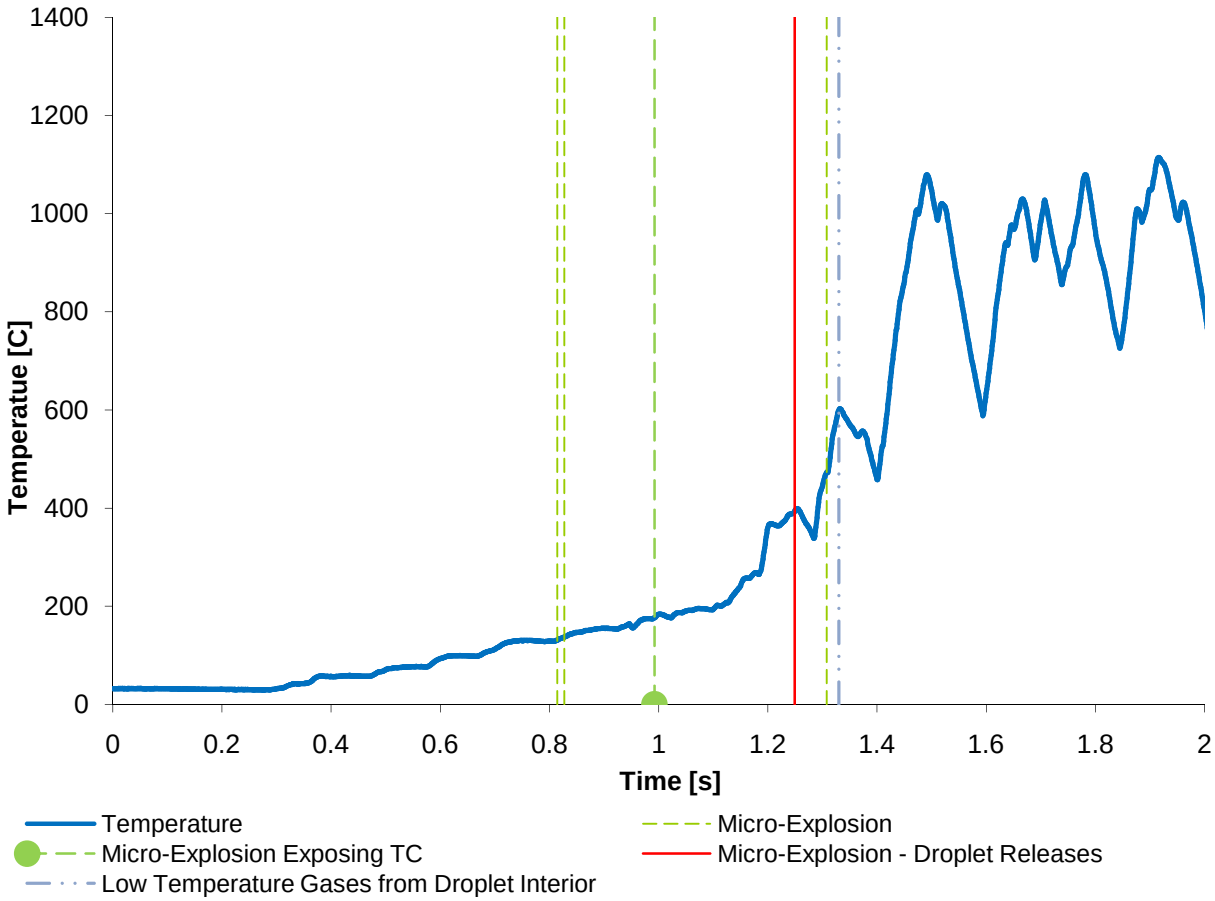

Figure 3-6: Temperature Time History – MSAR70-108 025-III (D_o=1.60 mm)

An interesting event occurs in Figure 3-5 when the droplet is released and begins a free fall. A micro-explosion occurs causing interior gases to be released and flow over the TC junction in the upward convective flow of the flame and result in a less than 0.1 second negative gradient before the flame temperature becomes dominant again. The lower micro-explosive rate of the fuel at the normalized height of 108 is presumed to be a function of temperature rather than the difference in A/F ratios at the different flame heights; which agrees with Kadota and Yamasaki (2002) that the micro-explosive rate is primarily a function of temperature and percent water content. If this is in fact the case than neglecting temperature increases associated with combustion, the pyrolysis of the

fuel can be assumed to have no consequence on the micro-explosive rate of the bitumen-in-water emulsion. However, it must be noted that second generation micro-explosions are much more rare at the normalized height of 50 than 108, which presents conflicting evidence against the previous statements. Temperature time histories for MSAR PPA/HFO for the normalized heights of 50 and 108 are shown in the Appendix.

Table 3-6 gives the temperature and waiting period for selected experimental runs of the MSAR-70% hydrocarbon fuel at the point of first occurrence of a stream and large-violent breakup at the normalized heights of 50 and 108. The waiting period is an empirical quantity defined as difference in time from the point at which the shielding plate begins to contract to the time of the first specified breakup.

Table 3-6: MSAR – 70% Hydrocarbon First Breakup Temperature and Waiting Period

	MSAR 70-50				MSAR 70-108			
Breakup Type	Test #	D_o (mm)	Temp. (°C)	Waiting Period (sec.)	Test #	D_o (mm)	Temp. (°C)	Waiting Period (sec.)
Stream	027-II	1.50	55.00	0.125	024-I*	1.70*	244.10*	1.025*
	026-II	1.52	50.50	0.150	025-I	1.50	79.00	0.700
	026-III	1.40	109.10	0.100	025-II	1.46	105.50	1.100
	026-IV	1.35	71.70	0.150	025-III	1.60	79.30	0.605
	026VI	1.04	212.70	0.100	025-IV	1.16	66.00	0.0348
Large-Violent	027-II	1.50	n/a	0.250	024-I*	1.70*	482.00*	2.020*
	026-II	1.52	63.70	0.350	025-I	1.50	137.60	1.100
	026-III	1.40	161.90	0.225	025-II	1.46	n/a	2.600
	026-IV	1.35	n/a	0.375	025-III	1.60	130.40	0.998
	026-VI	1.04	225.00	0.200	025-IV	1.16	144.00	0.283

*Test # 024-I is an outlier because its first large-violent breakup occurrence is an annihilation micro-explosion which results in a large waiting period and high core temperature at this first and only large-violent breakup occurrence

Table 3-6 indicates that the waiting period for a stream or large-violent breakup to occur is typically longer at the normalized height of 108 compared to 50. The magnitude at which the waiting period is higher is dependent on droplet initial diameter (D_o) and other unknown variables, e.g., fuel shell formation rate. The waiting period is longer for droplets with a larger initial diameter presumably because of the longer heating period associated with increased volume as indicated by the higher core temperatures at breakup of those droplets with smaller diameters. Large-Violent breakups occurring at droplet core temperatures less than 100°C is evidence that micro-explosion of the MSAR fuel is localized rather than initiating and propagating radially from the droplet's center.

3.5 Consequences of water content and volatile Hydrocarbons as the continuous phase in an MSAR emulsion

Tests were performed on neat bitumen for purposes of a control. The neat bitumen was found to exhibit some stream-like breakup properties, however, this is most likely attributed to the natural occurring water content present in bitumen and the wide range of volatility of the different hydrocarbons that make up the oil. The fact the neat bitumen did not exhibit localized or large-violent breakup type breakups supports previous conclusions that micro-explosion intensity is a function emulsified water volume. Figure 3-7 is a graph of a neat bitumen droplet's core temperature time-history at the normalized height of 50.

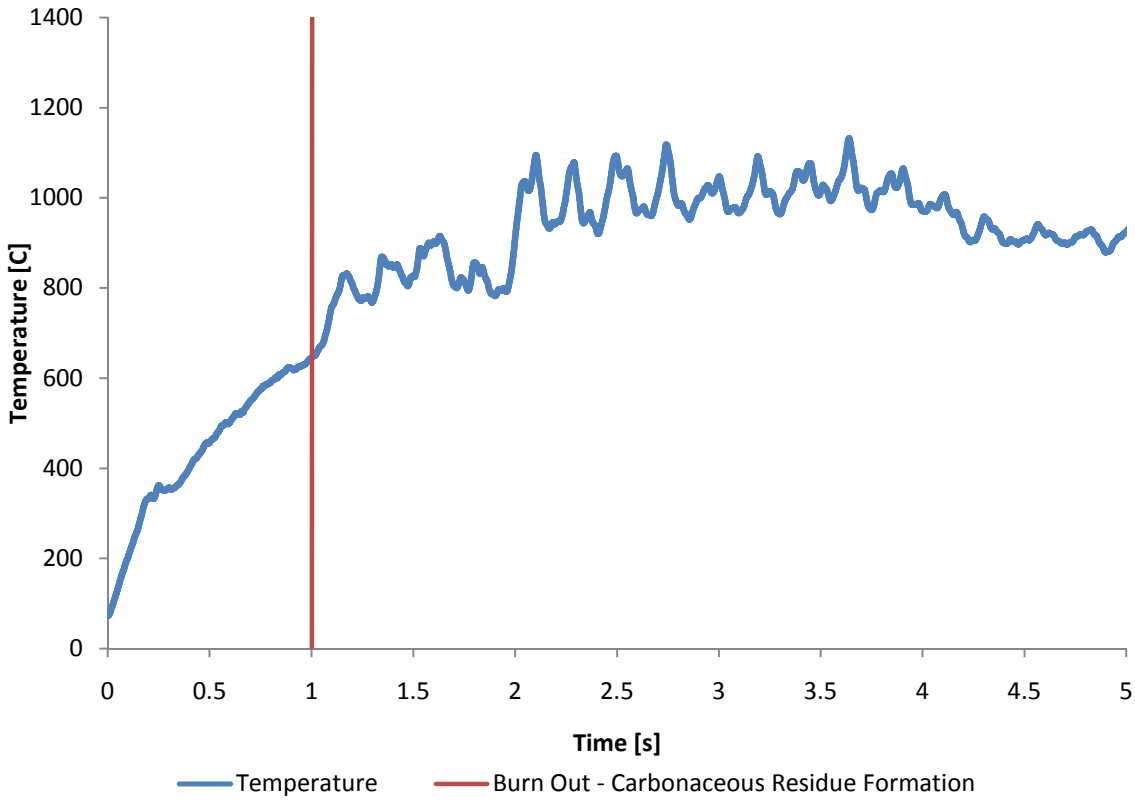

Figure 3-7: Temperature Time History – NEAT-50 026-II (D_o=0.942 mm)

Figure 3-7 indicates that neat bitumen burns with a normal regression curve as compared to the MSAR fuels. Additionally, neat bitumen combustion terminates with the formation of a carbonaceous residue on the thermocouple junction and rarely did an experimental run result in the release of the neat bitumen droplet from the thermocouple junction before complete burn out. Burning rate of the fuel is also much slower than that of the MSAR fuels. Table 3-7 below gives the waiting period for and temperature at the first occurrence of stream and large-violent breakups for selected experimental runs for MSAR-80% hydrocarbon and neat bitumen at the normalized height of 50.

Table 3-7: MSAR - 80% Hydrocarbon and Neat Bitumen First Breakup Temperatures and Waiting Periods

	MSAR 80-50				Neat Bitumen-50			
Breakup Type	Test #	D_o (mm)	Temp. (°C)	Waiting Period (seconds)	Test #	D_o (mm)	Temp. (°C)	Waiting Period (seconds)
Stream	026-II	1.25	56.10	0.125	026-I	1.520	n/a	0.100
	027-I	1.22	104.00	0.125	026-II	0.942	99.30	0.0265
	026-I	2.11	96.40	0.111	026-III	1.250	63.50	0.0868
	026-III	1.18	106.00	0.053	027-I	1.350	n/a	0.267
Large-Violent	026-II	1.25	245.90	0.447	026-I	1.520	n/a	n/a
	027-I	1.22	287.60	0.000	026-II	0.942	n/a	n/a
	026-I	2.11	n/a	n/a	026-III	1.250	n/a	n/a
	026-III	1.18	345.20	0.408	027-I	1.350	n/a	n/a

The waiting period for a stream breakup to occur for the neat bitumen in general is shorter than for the MSAR fuels as can be seen by comparing Tables 3-6 through 3-8. The temperature comparison between the neat bitumen and the MSAR fuels at the first

stream-breakup is not easily correlated based on the data obtained. Comparing Tables 3-6 and 3-7 it can be seen that the 20% water content MSAR fuel's large-violent breakups occur at greater temperatures than the MSAR fuel containing 30% water content. Presumably, there is greater heat removal with increased water content. Figure 3-8 below is a core temperature time-history for MSAR – 80% hydrocarbon at the normalized height of 50 for experimental run 026-III.

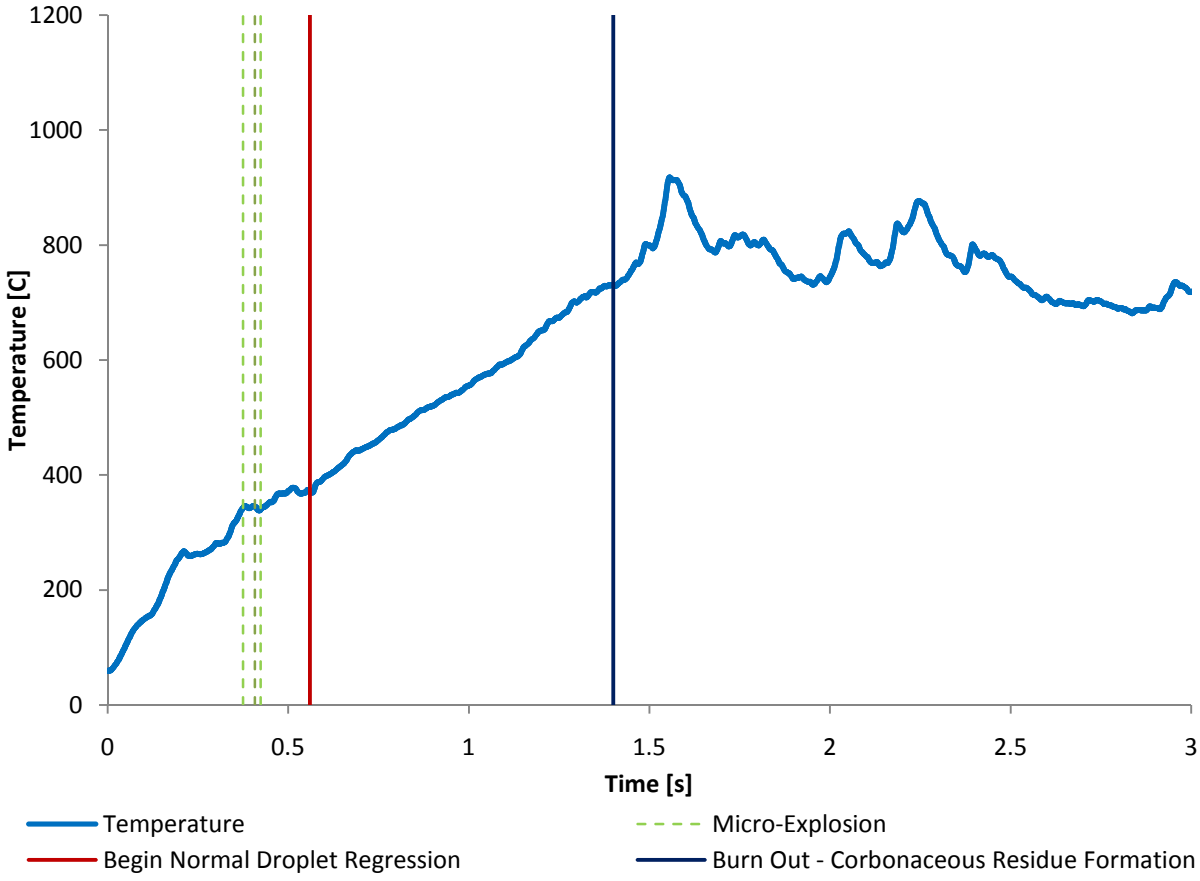

Figure 3-8: Temperature Time History – MSAR80-50 026-III (D_o=1.18 mm)

Test #026-III of the MSAR – 80% hydrocarbon fuel was one of the few experimental runs of the fuel that displayed a hybrid behavior between the emulsified fuel and the neat bitumen. Most displayed behavior consistent with the MSAR – 70% hydrocarbon fuel. As can be seen from Figure 3-3 the MSAR – 80% initially displays temperature time-history characteristics associated with disruptive burning, but after approximately 0.600 seconds into the test a normal droplet regression curve is present in Figure 3-3. Empirical evidence from the high-speed cameras also supports this sequence of events. It is appears that after the specified 0.600 seconds nucleation bubble growth ceases (regime four) possibly marking the complete vaporization of water from the parent droplet. With no trapped water to form super-heated heterogonous and/or homogenous nucleation sites within the droplet interior micro-explosions cease and normal droplet regression burning initiates. Furthermore, this experimental run culminated with the formation of a carbonaceous residue on the thermocouple junction. Approximately, 1/5 of the MSAR – 80% hydrocarbon runs ended with this occurrence. One last empirical observation to support these claims was the increased frequency of visible plumes surrounding the parent droplet. MSAR – 80% hydrocarbon's atomized satellite droplet size distributions are larger than those of MSAR – 70% hydrocarbon and MSAR – PPA/HFO. Future work is required to measure these satellite size distributions accurately. During breakups the ligaments of the fuel shell of the MSAR – 80% hydrocarbon can be seen. From these observations it is determined that the fuel shell is thicker for the MSAR – 80% hydrocarbon fuel as compared to the MSAR – 70% hydrocarbon and MSAR – PPA/HFO fuels. Finally, the micro-explosions of MSAR – 80% hydrocarbon fuel are determined to be the least intense of the other two MSAR fuels.

Table 3-8 below gives the temperature and waiting period for selected experimental runs of the MSAR - PPA/HFO fuel at the point of first occurrence of a stream and large-violent breakup for the normalized heights of 50 and 108.

Table 3-8: MSAR-PPA/HFO First Breakup Temperatures and Waiting Periods

	MSAR PPA/HFO-50				MSAR PPA/HFO-108			
Breakup Type	Test #	D_o (mm)	Temp. (°C)	Waiting Period (sec.)	Test #	D_o (mm)	Temp. (°C)	Waiting Period (sec.)
Stream	026-I	1.510	69.000	0.090	024-II	1.610	81.700	0.625
	026-III	0.965	201.500	n/a	024-III	1.330	105.600	1.025
	026-V	1.203	247.100	0.120	024-VI	1.630	80.500	0.525
	027-II	1.350	159.300	0.075	027-II	1.620	115.300	0.540
Large-Violent	026-I	1.510	117.600	0.175	024-II	1.610	198.000	1.350
	026-III	0.965	368.900	0.450	024-III	1.330	235.600	1.400
	026-V	1.203	249.600	0.225	024-VI	1.630	224.100	1.600
	027-II	1.350	202.400	0.300	027-II	1.620	233.000	n/a

Comparing Tables 3-6 and 3-8 one can see that the MSAR PPA/HFO fuel breakups occur at much greater temperatures than the MSAR – 70% hydrocarbon fuel. Generally speaking the waiting periods for MSAR PPO/HFO are shorter than for the MSAR – 70% hydrocarbon fuel, however the micro-explosive rate of the MSAR PPO/HFO fuel is greater compared to the 30% water content fuel. On the other hand MSAR – 70% hydrocarbon appears to have the greatest intensity of micro-explosions of all the fuels. MSAR - PPO/HFO has more intermittent visible plumes during its combustion than the MSAR -70% hydrocarbon. MSAR – PPA/HFO fuel, finally, has visibly greater surface tension than the MSAR – 70% hydrocarbon fuel.

3.6 Modeling

A simplified model is presented to model the breakup of an MSAR parent droplet as a result of micro-explosions associated with the three breakup regimes that have been presented. The model is based on Tankin and Li's (1987) model for sprays based on the

maximum entropy principle also known as information theory. Because we cannot intrinsically predict the behavior of a micro-explosion we must use probability to define droplet size and droplet velocity spaces. But we also do not know which of the probability distributions are most conservative from breakup to breakup so we must also incorporate the maximum entropy principle. Thus, the model simply looks to take the principles Tankin and Li used to model sprays based on these principles and apply it to the atomization that occurs during an instantaneous parent droplet breakup. The "blow holes", i.e., the openings in the parent droplet surface as a result of micro-explosion will be modeled as the nozzle exit, while the satellite droplets will be consistent of the liquid spray. Blow hole diameter increases with increasing breakup regime number. Li and Tankin's model obviously does not account for transient effects, e.g., changes in "nozzle diameter" as would be the case during the burning of an MSAR droplet, thus to be in accordance with Tankin and Li's model and for simplicity a quasi steady state condition within the MSAR burning process, i.e., the modeling of a single breakup with instantaneous blow hole diameter and breakup will be assumed in extrapolating over the model. To model the non-transient case as it relates to the MSAR droplet a triple integrand would be required to include changes in the droplet size and velocity spaces due to multiple breakups. Tankin and Li's model is a double integrand model including velocity and droplet diameter spaces. The author does not wish to consider at this juncture the modeling across multiple breakups that can occur less than one micro second apart from each other.

It is assumed there is no liquid sheet at the blow hole exit, but there is rather an instantaneous atomization of satellite droplets at the parent droplet exit. Consequently,

the source terms in Tankin and Li's constraint equations that are to be presented can be neglected. The source terms represent the positive or negative gradients associated with liquid droplet formation from the time of nozzle exit to final droplet formation; because satellite droplets are assumed to be already formed at their exit from the parent droplet the source terms will go to zero. Tankin and Li's (1987) statistical-optimization (maximum entropy principle) model based on the governing equations of mass, momentum and energy is presented below as it relates to a single micro-explosion of the MSAR fuel:

The first governing constraint is that of continuity or conservation of mass shown as Equation 4 below,

$$Mass: \sum_i \sum_j P_{ij} V_i \rho_l = \dot{m}_l + S_m \tag{4}$$

where P_{ij} is the number-based probability of the satellite droplet size at breakup distributed over the satellite droplet volume, V_i, and satellite droplet velocity, U_j spaces. ρ_l is the liquid density of the satellite droplets, which may be variable between satellite droplets but is assumed constant here. $\dot{n}$ is the rate at which satellite droplets exit the parent droplet blow hole and $\dot{m}_l$ is the rate of mass exiting the parent droplet. Finally, S_m is the mass source term which is neglected because no liquid sheet is assumed to form as a result of breakup. Li and Tankin non-dimensionalized their variables based on initial spray velocity, U_o, and mean droplet volume, V_m. The same will be done here to retain simplicity; however, U_o and V_m here will represent initial bulk satellite droplet velocity and mean satellite droplet volume distribution, respectively, where V_m is defined mathematically below

$$V_m = \frac{\dot{m}_l}{\rho_l \dot{n}} \tag{5}$$

Given this the droplet dimensionless velocity and volume are defined below as follows

$$\bar{U}_j = \frac{U_j}{U_o} \qquad \bar{V}_i = \frac{V_i}{V_m}$$

, where the over bar represents a non-dimensionalized quantity. Neglecting the source term, the non-dimensionalized conservation of mass equation is then

$$\text{Mass: } \sum_i \sum_j P_{ij}\, \bar{V}_i = 1 \tag{6}$$

The non-dimensionalized momentum and energy governing equations keeping with the representation in Equation 6 are as follows,

$$\text{Momentum: } \sum_i \sum_j \bar{P}_{ij} \bar{V}_i\, \bar{U}_J = 1 \tag{7}$$

$$\text{Energy: } \sum_i \sum_j P_{ij} \left(\bar{V}_i \bar{U}^2{}_j + B' K_i \bar{V}_i \right) = 1 \tag{8}$$

where K_i is the ratio of surface area, $A_{i,}$ to volume, $V_{i,}$ of the satellite droplets in size group i, defined as,

$$K_i = \frac{A_i}{V_i}$$

$B^{'}$ having the dimension of length is defined as

$$B' = \frac{2\sigma}{\rho_l U_o^2}$$

, where σ is the surface tension of the liquid satellite droplets. The optimization problem that is the maximum entropy principle by definition calls for one additional governing equation to complete the model to ensure the normalization constraint of the probability distributions, $P_{ij,}$ are not violated, which anyone familiar with the laws governing probability should recognize; the constraint is outlined below as Equation 9

$$\text{Normalization: } \sum_i \sum_j P_{ij} = 1 \tag{9}$$

As Li and Tankin (1987) point out there are an infinite set of probability distributions, P_{ij}, which satisfy Equations 6-9. Thus, the cost function known as the Shannon Entropy is needed and must be maximized within the constraints of Equations 6-9 in order to determine the probability distribution most certain to include all possible events within the constraints that would determine the satellite droplet sizes and velocities associated with the breakup of the MSAR droplet. There maybe information that is unknown that could affect which probability distributions is used to represent the breakup; maximizing the Shannon entropy ensures a probability distribution is chosen that includes this uncertainty. The Shannon Entropy is defined as follows

$$S = -k \sum_i \sum_j P_{ij} \ln P_{ij} \tag{10}$$

where *k* is a constant. The cost function, Equation 10, is maximized by applying the Karush-Kuhn-Tucker (KKT) optimality conditions to Equation 6-10. Doing so redefines the equations as a Langrangian Function in which langrage multipliers associated with the individual constraints must be solved for to determine the probability distribution that is of maximum entropy. Applying this method the probability distribution that represents that of maximum entropy can be given (Li and Tankin, 1987) as

$$P_{ij} = exp\left[-\alpha_o - \alpha_1 \overline{V}_i - \alpha_2 \overline{V}_i \overline{U}_j - \alpha_3 \left(\overline{V}_i \overline{U}_j^2 + B' K_i \overline{V}_i\right)\right] \tag{11}$$

where α_i (i = 0, 1, 2, 3) are the Lagrange multipliers associated with the individual constraints. Li and Tankin derive Equation 11 in their 1987 paper using the methods described above and thus it will not be repeated here. Equation 11 can now be applied to determine the probability of finding satellite droplets whose volume is between $\overline{V}_{n-1}$ and $\overline{V}_n$, and whose velocity is between $\overline{U}_{m-1}$ and $\overline{U}_m$ by evaluating the joint probability distribution below

$$P(\bar{V}_{n-1} < \bar{V} < \bar{V}_n,\ \bar{U}_{m-1} < \bar{U} < \bar{U}_m) =$$

$$= \sum_{\bar{V}_{n-1}}^{\bar{V}_n} \sum_{\bar{U}_{m-1}}^{\bar{U}_m} P_{ij}$$

$$= \sum_{\bar{V}_{n-1}}^{\bar{V}_n} \sum_{\bar{U}_{m-1}}^{\bar{U}_m} exp\left[-\alpha_o - \alpha_1 \bar{V}_i - \alpha_2 \bar{V}_i \bar{U}_j - \alpha_3 \left(\bar{V}_i \bar{U}_j^2 + B' K_i \bar{V}_i\right)\right] \quad (12)$$

Borrowing yet another observation from Tankin and Li it is generally regarded that sprays vary continuously rather than discretely, which would also be the case in a parent droplet breakup. Consequently, Equation 12 must be put into its integral form, which is done below

$$P(\bar{V}_{n-1} < \bar{V} < \bar{V}_n, \quad \bar{U}_{m-1} < \bar{U} < \bar{U}_m) =$$

$$\int_{\bar{V}_{n-1}}^{\bar{V}_n} \int_{\bar{U}_{m-1}}^{\bar{U}_m} \left(-\alpha_o - \alpha_1 \bar{V}_i - \alpha_2 \bar{V}_i \bar{U}_j - \alpha_3 \left(\bar{V}_i \bar{U}_j^2 + B' K_i \bar{V}_i\right)\right) d\bar{V} d\bar{U} \quad (13)$$

If we assume the satellite droplets exiting the parent droplet to be spherical we can simplify Equation 13 by representing the satellite droplet mean volume in terms of the mass mean diameter, D_{30},

$$V_m = \frac{\pi}{6} D_{30}^3$$

The non-dimensional volume can thus be represented in terms of the non-dimensional mass mean diameter as follows

$$\bar{V} = \left(\frac{D}{D_{30}}\right)^3 = \bar{D}_{30}^3 \quad (14)$$

where $\bar{D}$ is the normalized satellite droplet diameter. Differentiating Equation 14 gives,

$$d\bar{V} = 3\bar{D}^2 d\bar{D}$$

Finally, substituting Equation 13 and 14 into Equation 12 gives

$$P(\bar{V}_{n-1} < \bar{V} < \bar{V}_n, \quad \bar{U}_{m-1} < \bar{U} < \bar{U}_m)$$

$$= P(\bar{D}_{n-1} < \bar{D} < \bar{D}_n, \quad \bar{U}_{m-1} < \bar{U} < \bar{U}_m)$$

$$= \int_{\bar{D}_{n-1}}^{\bar{D}_n} \int_{\bar{U}_{m-1}}^{\bar{U}_m} 3\bar{D}^2 exp\left[-\alpha_o - \alpha_1 \bar{D}^3 - \alpha_2 \bar{D}^3 \bar{U}_j - \alpha_3 \left(\bar{D}^3 \bar{U}_j^2 + B\bar{D}^3\right)\right] \quad (15)$$

where

$$B = \frac{12}{We}$$

where We is the Weber number defined as

$$We = \frac{U_o^2 \rho_l D_s}{\sigma}$$

The Weber number defined here by Li and Tankin (1987) is not in its conventional form. The conventional Weber number defines the density as that of the gas medium in which the spray enters into and the difference in the gas and liquid medium velocities as the characteristic velocity, whereas here ρ_l is the density of the liquid medium or spray and U_o is (for our purposes) the satellite droplet initial velocity. Having given this disclaimer, we now define the joint probability density function (PDF) of the velocity and droplet size spaces as

$$f = 3\bar{D}^2 exp\left[-\alpha_o - \alpha_1 \bar{D}^3 - \alpha_2 \bar{D}^3 \bar{U}_j - \alpha_3 \left(\bar{D}^3 \bar{U}_j^2 + B' K_i \bar{D}^3\right)\right] \quad (16)$$

then Equation 15 becomes

$$\int_{\bar{D}_{n-1}}^{\bar{D}_n} \int_{\bar{U}_{m-1}}^{\bar{U}_m} f d\bar{D} d\bar{U} \quad (17)$$

Taking Equation 17 Li and Tankin (1987) note that for any specific droplet size, the PDF over the velocity space is a normal distribution about an average value. If Equation 17 is integrated over a known minimum and maximum velocity space then the droplet size distribution becomes

$$\frac{dN}{d\bar{D}} = \frac{3}{2}\left(\frac{\pi \bar{D}}{\alpha_3}\right)^{1/2} [\text{erf}(x_{max}) - \text{erf}(x_{min})] * exp\left[-\alpha_0 - \alpha_3 B \bar{D}^3 - \left(\alpha_1 - \frac{\alpha_2}{4\alpha_4}\right)\bar{D}^3\right] \quad (18)$$

where

$$x_{max} = \left(\overline{U}_{max} + \frac{\alpha_2}{2\alpha_3}\right)(\alpha_3 \overline{D}^3)^{1/2}$$

$$x_{min} = \left(\overline{U}_{min} + \frac{\alpha_2}{2\alpha_3}\right)(\alpha_3 \overline{D}^3)^{1/2}$$

and erf(x) is the error function.

Finally in accordance with Equation 15 the integral formulation of the governing constraints given in Equations 6-9 can be given as

$$\text{Mass: } \iint f\overline{D}^3 \, d\overline{U}d\overline{D} = 1 \tag{19}$$

$$\text{Momentum: } \iint f\overline{D}^3 \, d\overline{U}d\overline{D} = 1 \tag{20}$$

$$\text{Energy: } \iint f\,(\overline{D}^3\overline{U}^2 + B\overline{D}^2)d\overline{U}d\overline{D} = 1 \tag{21}$$

$$\text{Normalization: } \iint f\, d\overline{U}d\overline{D} = 1 \tag{22}$$

Li and Tankin's model can also be used to model the transient state as well as the steady state by replacing the mass mean diameter (MMD) by the Sauter mean diameter (SMD) thus incorporating droplet deformation with time and noting that the lagrange multipliers will need to be solved for continuously at each subsequent time interval.

3.6.1 Parent Droplet Nozzle Formulation Model

The following discussion and representation wishes to derive an equation to represent the force needed to breakthrough the parent droplet's fuel shell and form a blow hole as it pertains to the case where a single satellite droplet exits the parent droplet's surface in a regime one breakup, i.e., stream breakup. If we are to model the parent droplet as a bubble with fuel shell thickness, *t*, and assume this thickness is negligible then the pressure differential across the fuel shell between the internal matter and atmosphere becomes

$$\Delta P_p = \frac{2\sigma}{D_p} \tag{23}$$

,where D_p is the parent droplet diameter. Now, if we consider a satellite droplet of diameter, D_s, exiting the parent droplet's surface from a circular opening in the fuel shell equal in area to

$$A_n = \frac{\pi}{4} D_s^2 \tag{24}$$

then the pressure differential across this opening in the parent's droplet surface is equal to

$$\Delta P_s = \frac{1}{2} \rho_l U_o^2 \tag{25}$$

, where ρ_l is the liquid density of the satellite droplet and U_o is the initial velocity of the satellite droplet at exit. If we were to neglect the presence of an exiting satellite droplet then the pressure differential across an area A_n at the parent droplet's surface is merely the result of surface tension which can be defined as follows

$$\Delta P_n = \frac{2\sigma}{D_s} \tag{26}$$

Then equating and rearranging Equations 25 and 26 the absolute minimum satellite droplet velocity needed to breakthrough a portion of the fuel shell equal in area to A_n at the parent droplet's surface is equal to

$$U_{min} = \left(\frac{4\rho_l \sigma}{D_s}\right) \tag{27}$$

Then the force required to breakthrough the fuel shell surface can be defined as follows

$$F_s = \rho_l D_s^2 U_{min}^2 = \sigma D_s We \tag{28}$$

This model neglects the force of any vapors exiting the blow hole that may increase the pressure differential across the opening in the parent droplet's surface and is not easily applied to regime two and three breakups of the MSAR droplet. However, the formulation may be useful in modeling the early stages of the MSAR burning process

when most breakups consist of single satellite droplet expulsion and a rapid recover of the fuel shell at the parent droplet’s surface.

CHAPTER 4: CONCLUSIONS AND RECCOMENDATIONS

4.1 Summary and Conclusions

Micro-explosion since its discovery by Ivanov and Nefedov in 1965 has been an involved, but extremely promising and interesting point of study within the combustion community. Micro-explosion stems from combustion of fuels that are composed of a non-volatile liquid fuel emulsified with a volatile liquid primarily but not limited to water. The most prevalent in use emulsified fuels to date our water-in-oil (W/O) and oil-in-water emulsions (O/W). The benefits of micro-explosion were also realized early on being found to contribute to increased combustion efficiency and emission reduction. Great progress has been made since then in understanding the phenomenon, however, still more progress is needed in order to utilize and model the combustion of micro-explosive fuels effectively.

Dwindling conventional oil resources marked by exponential consumption has caused industry to look elsewhere into alternative oils such as bitumen from Oil Sands. Beginning with Orimulsion researchers discovered that combining the heavy oil with water in an O/W type emulsion was the most effective way to limit the fuels effects on the environment and increase its efficiency by means of micro-explosion. The next generation of bitumen-in-water emulsions, MSAR, began being produced by Quadrise Canada Corporation in the early 1990s.

Experiments were performed using a methane diffusion flame test set-up to combust MSAR fuel droplets. The MSAR droplet core temperatures were monitored during experimentation by their suspension on a thermocouple junction. Qualitative data

was collected by means of two high-speed cameras one being monochrome and the other color at 1808 fps and 1200 fps, respectively.

MSAR proved to have three distinct breakup regimes that the fuel cycled between during combustion: stream breakups, localized breakups and large-violent breakups. The different properties that were discovered to mark each of theses breakup regimes, e.g., breakup velocities and temperatures, in conjunction with the disruptive burning regimes themselves makes the MSAR droplet combustion extremely difficult to optimize and model. The effects these different magnitudes have on modifying the behavior of liquid-gas flow and fuel-air mixing within a combustor will need to be determined. As part of this process the MSAR fuel droplet core temperatures at breakup (micro-explosion) were monitored and documented.

Previous investigations (outlined in Sec. 1.3) have postulated and shown evidence that a viscous fuel shell forms on the exterior of emulsified fuel droplets trapping water vapor eventually leading to rupturing of the droplet, i.e., micro-explosion. The experimental evidence obtained as a result of this investigation supports these conclusions. However, it has been concluded that Zeng's model of a single bubble nucleation growth from the origin of the emulsified fuel droplet is not applicable for the modeling a MSAR droplet in a combustor. As a result of Hill's spherical vortices that form within the interior of the MSAR droplet the micro-explosive nature of an MSAR droplet is localized. From this, it is postulated that not only does a fuel shell form on the exterior of an MSAR droplet, but that pockets or chambers containing this fuel shell may also form within the droplet interior. These pockets serve as homogeneous nucleation sites for the onset of micro-explosion.

Dryer (1977) concluded that heterogeneous nucleation will inhibit micro-explosion as a result of agglomeration of water at metal interfaces, however it has been determined that this criteria does not apply to the MSAR fuel. In fact, heterogeneous nucleation is shown to enhance the intensity as well as the frequency of micro-explosion. Heterogeneous sites result in micro-explosions that occur at a lower temperature and pressure (pressure effects were not investigated in this study).

The MSAR burning process can be broken up into three distinct processes:

1. Heating Period and Viscous Fuel Shell Formation
2. Cyclic Period (Repeats Until Termination Step 3)
    a. Bubble Nucleation Growth and Fuel Shell Expansion
    b. Regime 1-3 Micro-Explosive Breakups
    c. Fuel Shell Reformation
3. Annihilation Micro-Explosion and/or burn out

The annihilation Micro-Explosion results in such fine atomization of the fuel droplet that Step 2c cannot occur and the cycle outlined in Step 2 is broken. The large surface area exposure of the remaining fuel volume resultant from the annihilation micro-explosion results in rapid vaporization and complete combustion of the remaining fuel.

Satellite droplets were found to produce second generation micro-explosions. Micro-exploding satellite droplets were measured with diameters less than 100 microns. Satellite droplet velocities were also measured to give an indication of the velocity distributions that maybe associated with micro-explosion. The maximum average velocities of satellite droplets resultant from stream, localized and large-violent breakups were measured for the three MSAR fuels studied. General trends showed that a decrease

in water content from 30% to 20% of the MSAR fuel resulted in breakup velocities that decreased in magnitude. The velocity data obtained was inconclusive to make any definitive comparisons between the breakup velocities of the MSAR PP/HFO fuel and the MSAR – 70% hydrocarbon fuel. Breakup velocities were found to be greater for the conditions associated with the fuel burning at a height that was approximately at the peak of the methane diffusion flame as opposed to a position closer to the flame's origin.

The MSAR fuels were burned at two separate heights within the methane diffusion flame. The heights were non-dimensionalized by the flame port diameter of 4 mm giving magnitudes of 50 and 108, respectively, with the height of 108 being approximately the maximum flame height. The change in air-fuel ratio at the different heights was determined to have no consequence on the micro-explosive intensity or micro-explosive rate of the MSAR fuels. The difference in air-fuel ratio however was consequential on the ignition delay and burning rate of the satellite droplets released due to micro-explosion. Temperature differences at the varying heights on the other hand were consequential on micro-explosion properties with micro-explosive rates being increased at the normalized height of 50 where greater average temperatures were present.

Three MSAR fuels were tested one containing 20% water content, one with 30% water content and a third using two unknown high volatility hydrocarbon as the continuous phase in place of water (MSAR – PPA/HFO). As with previous studies micro-explosive intensity and rate was shown to be directly correlated with water content. Micro-explosive frequency and intensity of the MSAR 30% water content fuel was the greatest followed by that of the MSAR PPA/HFO fuel, although breakup velocity

data was inclusive in supporting this qualitative observation. The MSAR 20% water content fuel had the thickest fuel shell of the three fuels observed through qualitative observations. The MSAR PPA/HFO fuel had the largest waiting period until first occurrence of a micro-explosion. The long waiting period of the MSAR PPA/HFO fuel as would be expected aligned itself with the highest droplet core temperatures at the first occurrence of micro-explosion followed by that of the MSAR 20% water content fuel having the second largest waiting period and highest temperatures at its first occurrences of micro-explosion.

Two simple models for the prediction of micro-explosive events were presented. The first model is based on Tankin and Li's (1988) model for sprays. The model is extrapolated in its use of maximum entropy principle also known as information theory to predict satellite droplet size and velocity joint probability density distributions resultant from a micro-explosion, modeling the "blow hole" in the parent droplet surface fuel shell as the nozzle exit and the satellite droplets as being consistent with the spray medium. More detailed measurements of size and velocity satellite droplet distributions associated with a micro-explosion will need to be obtained in order to validate the model for use with MSAR fuel; if found valid the model can be used to predict micro-explosive satellite droplet velocity and size distributions during the burning of an MSAR droplet. The second model predicts the force needed to breakthrough the parent droplet surface fuel shell for a stream type breakup based on the pressure drop across an opening in the fuel shell equal in diameter to a satellite droplet that is to breakthrough. If determined valid the model can be applied in the context of a more involved model to determine the minimum nucleation energy required for a micro-explosion to occur and be a starting

point for modeling micro-explosions as a function of homogeneous and heterogeneous nucleation bubble growth rates and energy by equating these values to satellite droplet kinetic energy or momentum. As a final note, correlating micro-explosion occurrence to the limit of super heat of water maybe proven to be too conservative of approach because the model will neglect stream and localized breakup occurrences that occur at temperatures lower than that of the limit of superheat of water.

The main contribution of this work was to provide qualitative and quantitative data and evidence that advances the understanding and knowledge base for bitumen-in-water emulsion combustion. These results contribute to the process of trying to understand the micro-explosive phenomenon taking place.

4.2 Recommendations and Future Work

Observations of the qualitative evidence and quantitative temperature data showed that heterogeneous nucleation sites, i.e., locations where the MSAR fuel was in contact with the thermocouple interface, resulted in micro-explosions that occurred at lower temperatures and with increased frequency. From this it is postulated that adding metal powders or more specifically metal nano-particles, e.g., aluminum or magnesium, as is done in solid rocket propellants will provide for such heterogeneous nucleation sites within the MSAR fuel droplet. It is presumed this addition will result in the MSAR fuel micro-exploding at reduced temperatures or increased rates at constant temperature. Future work should be conducted to determine the validity of this argument and if proven valid then proceed to determine the optimal ppm of the metal nano-particles to be added to the MSAR fuel. Also moving forward the consequences of the addition of the metal nano-particles would need to be accessed such as agglomeration of liquids around the

metal particles or their buildup within a combustor overtime. The agglomeration of water around the metal nano-particles maybe found to be beneficial as opposed to detrimental.

Additional future work should include velocimetry techniques for the measurement of droplet breakup velocities, measurement of droplet size distributions during breakup using a particle analyzer, observation and measurement of droplet-droplet interactions and collisions, and study of the behavior and micro-explosive tendencies of satellite droplets. Because of the large quantity of hydrocarbon fractions contained in bitumen, pyrolysis and spectroscopic studies of the MSAR fuel are warranted as well to determine the consequences individual species may have on emissions or other parameters. Finally, future work should be conducted to either validate or invalidate the "Parent Droplet Nozzle Formulation Model" presented in this paper. The optimal goal in studying micro-explosive fuels must be to optimize micro-explosion intensity and frequency. Once these areas have been explored, a more in depth investigation can be more easily conducted on bulk vaporization and burning rates of the MSAR fuel and emulsified fuels in general.

APPENDIX

MSAR PPA/HFO Temperature Time-Histories:

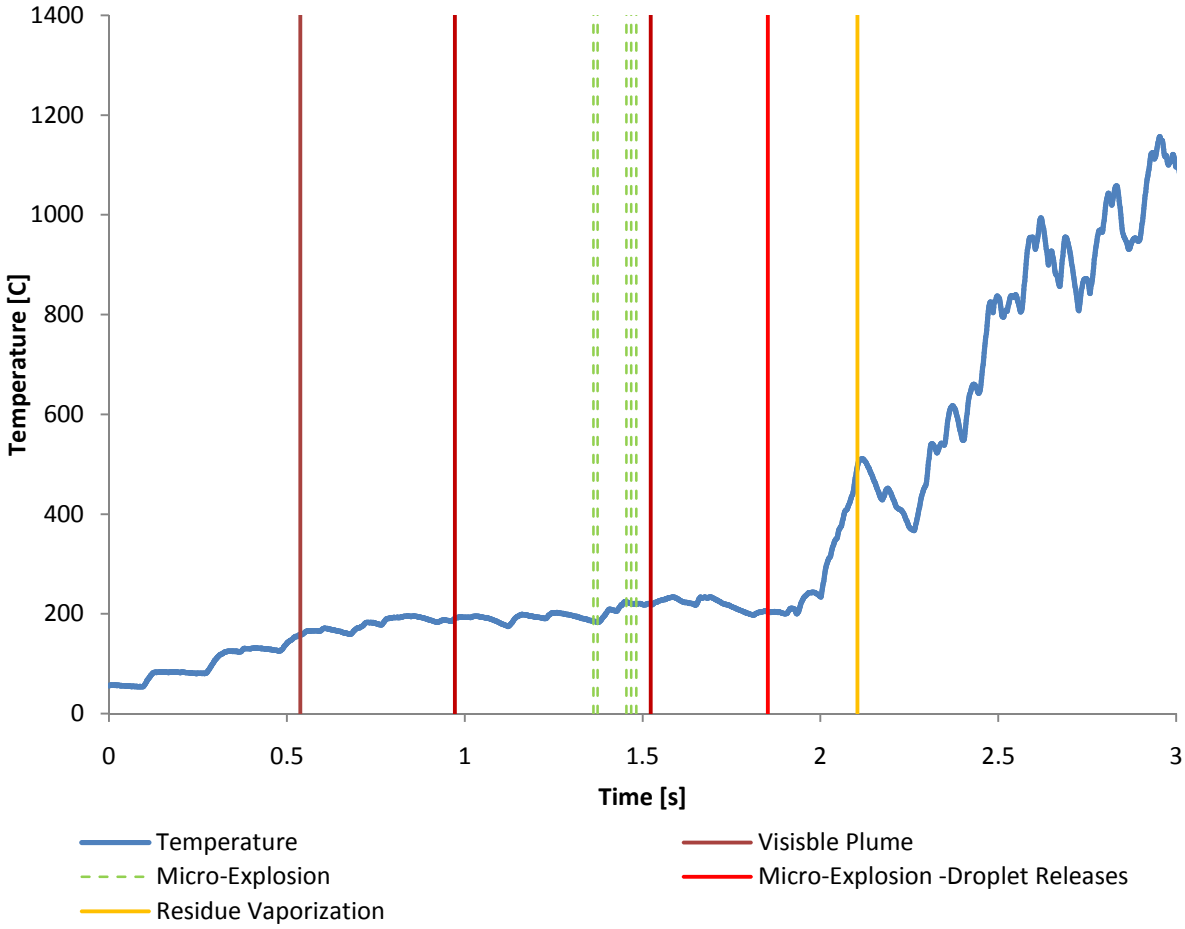

Figure A-1: Temperature Time History – MSAR PPA/HFO-108 024-VI (Do=1.62 mm)

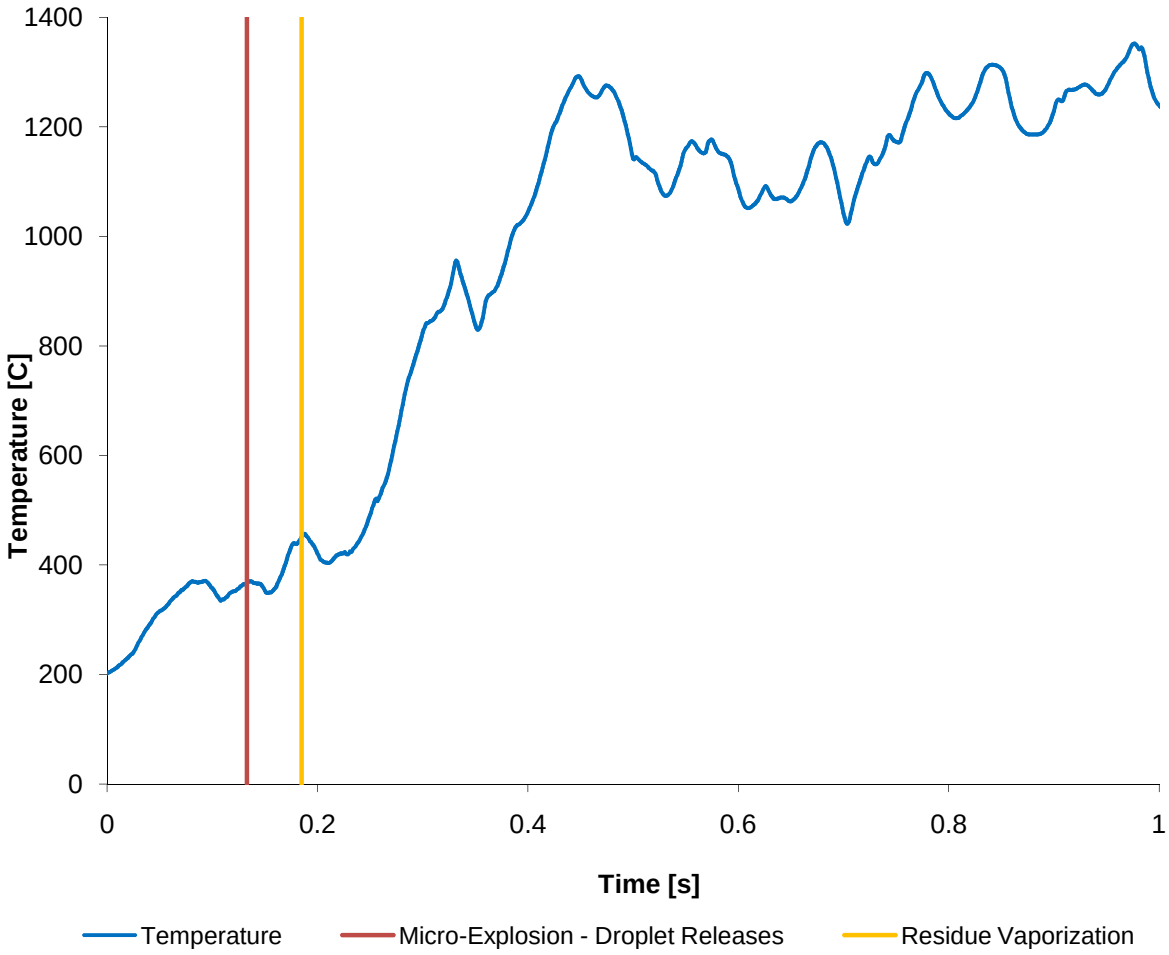

Figure A-2: Temperature Time History – MSAR PPA/HFO-50 026-III (Do=0.965 mm)

REFERENCES

Ali, S. M. Farouq (2003). Heavy Oil-evermore mobile. *Journal of Petroleum Science and Engineering, 37, 5-9.* Retrieved August 15, 2006, from Science Direct database.

Avedesian, C. T. & R. P. Andres (1978). Bubble Nucleation in Emulsions and Mixtures. *Abstracts of Papers of the American Chemical Society*, 176 MAR, 121-121.

Avedisian, C. T. & I. Glassman (1981). High Pressure Homogeneous Nucleation of Bubbles within the Super Heated Binary Liquid Mixtures. *Journal of Heat Transfer,* 103 (2), 272-280.

Avedisian, C. T.& M. Fatehi (1987). An Experimental Study of the Leidenfrost Evaporation Characteristics of Emulsified Liquid Droplets. *Int. J. Heat and Mass Transfer*, 31 (8), 1587-1603.

Barker, William G. (2006). Gasoline Prices, Macroeconomics and Sustainable Transportation. *85th Annual Meeting of theTransportation Research Board* Washington, D.C January 24, 2006.

Bitumenes Orinico S.A. (2006). BITUMENES ORINOCO, S.A., THE POWER OF SUSTAINABLE DEVELOPMENT. *Sovereign Publications Limited.* Retrieved February 4, 2007 from http://www.sovereign-publications.com/bitumene.htm.

Cho, P., C. K. Law, & M. Mizomoto (1991). Effect of Pressure on the Micro-Explosion of water/oil Emulsion Droplets over a Hot Plate. *Journal of Heat Transfer,* 113 (1), 272-274.

Czarnecki J., Hamza H., Masliyah J., Xu ZH, & Zhou ZJ. (2004). Understanding water-based bitumen extraction from Athabasca oil sands. *Canadian Journal of Chemical Engineering*, 82 (4), 628-654.

Dryer, F. L. (1977). Water Addition to Practical Combustion Systems – Concepts and Applications. *Sixteenth Symposium (International) on Combustion,* 279-295.

Energy Information Administration (2006). Retrieved October 28, 2006 from http://tonto.eia.doe.gov

Faeth, G. M. (1977). Current Status of Droplet and Liquid Combustion. *Progress in Energy and Combustion Sciences*, 3, 191-224.

Fu, Wei Bia, Ling You Hou, Lipo Wang, & Fan Hua Ma (2002). A Unified Model for the Micro-Explosion of emulsified Droplets of Oil and Water. *Fuel Processing Technology.* 79, 107– 119.

Greene, David L., & John DeCicco (2000). Energy and Transportation Beyond 2000. *Transportation Research Board*. Retrieved January 17, 2007 from http://www.nationalacademies.org/trb/publications/millennium/00032.pdf

Hall, Peter (1996). The Future of the Metropolis and its Form. *Regional Studies,* Vol. 31.3, 211-220.

Hubbert, M. King (1956). Nuclear Energy and the Fossil Fuels. *The American Petroleum Institute,* Spring Meeting of Southern District Division of Production, Plaza Hotel, San Atonio, TX March 7-9, 1956.

Hubbert, M. King (1981). The World's Evolving Energy System. *American Journal of Physics,* 49 (11), 1011-1029.

Ivanov, V. M. & P. I. Nefedov (1965). Experimental Investigation of the Combustion Process of Natural and Emulsified Fuels. *NASA Scientific and Technical Publications from Trudy Instituta Goryacikh Iskopayemykh,* 19, 35-45.

Kadota, T. & H. Yamasaki (2002). Recent Advances in the Combustion of Water Fuel Emulsion. *Progress in Energy and Combustion Science,* 28, 384-404.

Kuo, Kenneth Kuan-yun (1986). Principles of Combustion. New York: John Wiley & Sons, Inc.

Law, C. K. (1977). A Model for the Combustion of Oil/Water Emulsion Droplet. *Combustion and Science Technology,* 17, 29-38.

Law, C. K, C. H. Lee, N. Srinivasan (1980). Combustion Characteristics of Water-in-Oil Emulsion Droplets. *Combustion and Flame,* 37, 125-143.

Law, C. K. (1982). Recent Advances in Droplet Vaporization and Combustion. *Progress in Energy and Combustion Sciences,* 8 (3), 171-201.

Lasheras, J. C., A. C. Fernadez-Pello, & F. L. Dryer (1979). Initial Observation of the Free Droplet Combustion Characteristic of Water-in-Fuel Emulsions. *Combustion and Science Technology,* 21, 1-14.

Li, Xianguo & Richard S. Tankin (1988). Derivation of Droplet Size Distribution in Sprays By Using Information Theory. *Combustion Science and Technology,* 60, 345-357.

Mawdsley, John P. Jeol, & Mikhareva, Jenny, & Tennison, Joel (2005). The Oil Sands of Canada. *Raymond James Financial Ltd.*

Marcano, N., M. Pourkashanian, & A. Williams (1990). The Combustion of bitumen-in-water Emulsions. *Fuel,* 70 (8), 917-923.

Masliyah J., Z. J. Zhou ZJ, Z. H. Xu, J. Czarnecki , H. Hamza (2004). Understanding Water Based Bitumen Extraction from the Athabasca Oil Sands. *Canadian Journal of Chemical Engineering,* 82 (4), 628-654.

Miller, C. A. and Srivastava, R. K., 2000, The combustion of Orimulsion and its generation of air pollutants. *Prog. Energy Combust. Sci*., 26, 131-160.

Namba, Kunihiko & Kyoki Kimoto (2000). Ignition and Combustion Behavior of Asphalt/Water Emulsified Fuels. *JSME International Journal: Series B,* 43 (3), 478-484.

National Energy Board (2004). Canada's Oil Sands: Opportunities and Challenges to 2015. *National Energy Board,* Retrieved February 3, 2007 from http://www.neb-one.gc.ca/clf-nsi/rcmmn/hm-eng.html.

Permanu, Subodhsen, Barry B. Pruden, & Parviz Rahimi (1999). Molecular Weight and Specific Gravity Distributions for Athabasca and Cold Lake Bitumens and Their Saturate, Aromatic, Resin, and Asphaltene Fractions. *Ind. Eng. Chem. Res., 38,* 3121-3130.

Quadrise Canada Corporation (2007). What is MSAR? *Quadrise Limited.* Retrieved December 27, 2007 from http://www.quadrisecanada.com/msar.html.

Schutte, Robert, Gordon R. Thompson, Kingsley K. Donkor, M. John M. Duke, Roger Cowles, Xiu Ping Li, & Byron Kratochvil (1999). Estimation of particle size distribution in Athabasca oil sands by indirect instrumental neutron activation analysis. *Can. J. Chem.*, 77, 1626–1637.

Segawa, Daisuke, Hiroshi Yamasaki, Toshikazu Kadota, Hidemitsu Tanaka, Hiroshi Enomoto, Mitsuhiro Tsue (2000). Water Coalescence in an Oil-in-Water Emulsion Droplet Burning Under Microgravity. *Proceedings of the Combustion Institute,* 28, 985-990.

Sinha, Kumares C. (2003). Sustainability and Urban Public Transportation. Journal of Transportation Engineering © ASCE, JULY/AUGUST 2003, 331-341.

Shim, G. E., Rhee SM, Ahn KH, Chung SB (2006). The Relationship Between the Characteristics of transportation energy consumption and urban form. *Annals of Regional Science,* 40 (2), 351-367.

Tsue M, Segawa D, Kadota T, Yamasaki H (1996). Observation of sooting behavior in an emulsion droplet flame by planer laser light scattering in microgravity. *Proceedings of the 26th Symposium (International) on Combustion. The Combustion Institute,* 1251–1258.

Wang, C. H., X. Q. Liu and C. K. Law. Combustion and Microexplosion of Freely Falling Multicomponet Droplets. *Combustion and Flame,* 56, 175-197.

Wikipedia (2007). M. King Hubbert. *Wikipedia Foundation Inc.* Retrieved January 17, 2007 from http://www.wikipedia.org/

Williams, Alan & M. Pourkashanian (1987). The Combustion of bitumen-water Mixtures. *Journal of the Institute of Energy,* 60 (45), 209-211.

Yamasaki H, Kadota T, Segawa D, Tsue M (1998). Time histories of water content in a burning an emulsified fuel droplet. *Trans Jpn Soc Mech Engr,* 64 (618), 562–567.

Zeng, Yangbing & Chia-fon F. Lee (2007). Modeling droplet breakup Processes under Micro-Explosion Conditions. *Proceedings of the Combustion Institute,* 31, 2185–2193.